NASA NASA CR 166664

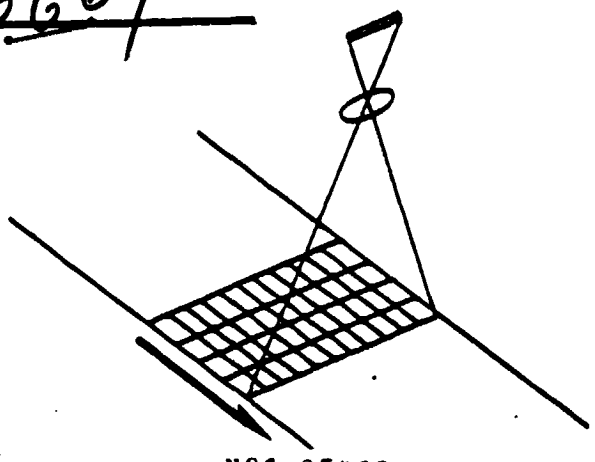

(NASA-CR-166664) MULTISPECTRAL RESOURCE SAMPLER (MRS): PROOF OF CONCEPT STUDY ON ATMOSPHERIC CORRECTIONS. DETERMINATIONS OF ATMOSPHERIC OPTICAL PARAMETERS USING THE MULTISPECTRAL RESOURCE SAMPLER (Operations G3/43

N81-25463

Unclas
28182

MRS: "PROOF-OF-CONCEPT" STUDY ON ATMOSPHERIC CORRECTIONS,

DETERMINATION OF ATMOSPHERIC OPTICAL PARAMETERS USING THE MULTISPECTRAL RESOURCE SAMPLER

By
Dr. Robert E. Turner
December 1979

PREPARED FOR
NASA—
GODDARD SPACE FLIGHT CENTER
GREENBELT, MD. 20771

BY
ORI, INC.
1400 SPRING ST.
SILVER SPRING, MD 20910

GSFC

UNCLASSIFIED

SECURITY CLASSIFICATION OF THIS PAGE (When Data Entered)

REPORT DOCUMENTATION PAGE		READ INSTRUCTIONS BEFORE COMPLETING FORM
1. REPORT NUMBER TR 1652	2. GOVT ACCESSION NO.	3. RECIPIENT'S CATALOG NUMBER
4. TITLE (and Subtitle) MRS, "Proof-of-Concept" on Atmospheric Corrections Determination of Atmospheric Optical Parameters Using the Multispectral Resource Sampler		5. TYPE OF REPORT & PERIOD COVERED Final 5/15/79 - 1/15/80 6. PERFORMING ORG. REPORT NUMBER
7. AUTHOR(s) Dr. Robert E. Turner		8. CONTRACT OR GRANT NUMBER(s) NAS5-25606 Subcontract #7102
9. PERFORMING ORGANIZATION NAME AND ADDRESS ORI, Inc. 1400 Spring Street Silver Spring, MD. 20910		10. PROGRAM ELEMENT, PROJECT, TASK AREA & WORK UNIT NUMBERS
11. CONTROLLING OFFICE NAME AND ADDRESS NASA-GSFC Code 942 Greenbelt, MD. 20771		12. REPORT DATE DECEMBER 1979 13. NUMBER OF PAGES 66
14. MONITORING AGENCY NAME & ADDRESS (if different from Controlling Office) ORI, Inc. 1400 Spring Street Silver Spring, MD. 20910		15. SECURITY CLASS. (of this report) UNCLASSIFIED 15a. DECLASSIFICATION/DOWNGRADING SCHEDULE

16. DISTRIBUTION STATEMENT (of this Report)

25 copies to Dr. Charles Schnetzler
Code 942
NASA-GSFC
Greenbelt, MD. 20771

17. DISTRIBUTION STATEMENT (of the abstract entered in Block 20, if different from Report)

18. SUPPLEMENTARY NOTES

Dr. Turner, of Science Applications, Inc., is a subcontractor to ORI, Inc. on this contract.

19. KEY WORDS (Continue on reverse side if necessary and identify by block number)

OPTICAL THICKNESS	VISUAL RANGE	TRANSMITTANCE
RADIATIVE TRANSFER	HAZE	AEROSOL
MULTISPECTRAL	BI-DIRECTIONAL	PATH RADIANCE
REMOTE SENSING	SATELLITE SIMULATION	

20. ABSTRACT (Continue on reverse side if necessary and identify by block number)

An investigation has been performed to determine which mathematical algorithms should be used in the calculation of atmospheric optical parameters using the Multispectral Resource Sampler (MRS) sensor. A simulation of the MRS sensor was performed using a radiative-transfer model. The simulation provides the spectral radiance at the satellite sensor in terms of various atmospheric parameters, such as optical thickness, solar zenith angle, nadir view angle, relative azimuth angle, bi-directional

DD FORM 1 JAN 73 1473 EDITION OF 1 NOV 65 IS OBSOLETE
S/N 0102-014-6601

UNCLASSIFIED

SECURITY CLASSIFICATION OF THIS PAGE (When Data Entered)

reflectance of the target, background albedo, and wavelength.

Atmospheric correction algorithms were also developed for the determination of the total spectral optical thickness of the atmosphere for: 1) homogeneous (horizontal) hazy atmospheres, with diffuse targets; 2) inhomogeneous (horizontal) hazy atmospheres with diffuse targets; and, for, 3) homogeneous (horizontal) hazy atmospheres with non-diffuse targets. It was demonstrated, with numerous plots, that if the goniometric (angular) properties of a neighboring pair of targets are known then the spectral optical thickness of the atmosphere can be determined using the MRS sensor. Conversely, it was also shown that if one knows the optical properties of the atmosphere for a specified area then the bi-directional reflectance distribution function of the targets can be determined.

As a result of this investigation, it was concluded that the MRS sensor can be a valuable new device for the multispectral remote sensing of Earth's surface. Specific recommendations were made for more detailed investigations of inhomogeneous atmospheres and general bi-directional reflectance distribution functions.

PREFACE

The Multispectral Resource Sampler (MRS) "Proof-of-Concept" Study is intended to be a comprehensive analysis of the corrections that must be applied to MRS data to allow for atmospheric correction factors and the variability of bidirectional reflectance from the scene.

This study was initiated by Dr. Charles Schnetzler of NASA Goddard Space Flight Center, and was performed by ORI, Inc. Space Data and Systems Division with Mr. Charles W. Aitken coordinating the efforts of ORI's consultants.

The complete study results are reported in five separate volumes which have the following titles and authors:

DETERMINATION OF ATMOSPHERIC OPTICAL PARAMETERS USING THE MULTISPECTRAL RESOURCE SAMPLER, by Dr. Robert E. Turner, Science Applications, Inc.

ATMOSPHERIC CORRECTION USING AN ORBITAL POINTABLE IMAGING SYSTEM By Dr. Philip N. Slater, University of Arizona

A SIMULATION ANALYSIS OF BIDIRECTIONAL REFLECTANCE PROPERTIES AND THEIR EFFECTS ON SCENE RADIANCE--IMPLICATIONS FOR THE MRS, By Dr. James A. Smith, Colorado State University

MRS LITERATURE SURVEY OF BIDIRECTIONAL REFLECTANCE, By Dr. James A. Smith, Colorado State University

MRS LITERATURE SURVEY OF ATMOSPHERIC CORRECTIONS By, Dr. Philip N. Slater, University of Arizona

ORI, Inc. would like to acknowledge the invaluable assistance of the following people who helped in the performance of this study:

Dr. P.N. Slater (Principal Investigator Atmospheric Corrections)	University of Arizona
Gen. R. S. Browning	University of Arizona
Dr. B. M. Herman	University of Arizona
Mr. S. J. Martinek	University of Arizona
Dr. R.A. Schowengerdt	University of Arizona
Dr. J. A. Smith (Principal Investigator Bidirectional Reflectance)	Colorado State University
Mr. K. J. Ranson	Colorado State University
Ms. J. A. Kirchner	Colorado State University
Dr. R. E. Turner (Principal Investigator Atmospheric Corrections)	Science Applications, Inc.

ORI
Silver Spring, Maryland 20910

DETERMINATION OF ATMOSPHERIC OPTICAL PARAMETERS USING THE MULTISPECTRAL RESOURCE SAMPLER

DECEMBER, 1979

PREPARED BY:
DR. ROBERT E. TURNER
SCIENCE APPLICATIONS, INC.

SUBCONTRACTOR TO:
ORI, INC.
SILVER SPRING, MARYLAND

FOREWORD

The NASA-designed Multispectral Resource Sampler sensor is an entirely new device for the multispectral remote sensing of Earth's resources. It has many advantages over existing sensor systems but the most important advantage from the atmospheric correction point of view is its pointability. The sensor can be set to receive radiation from a particular target or pair of targets for many nadir view angles. This fact is particularly advantageous because it allows an investigator to determine the aerosol optical thickness of the atmosphere.

Science Applications, Inc. was selected as a subcontractor to ORI to perform satellite simulations of the MRS satellite radiances and to develop algorithms which can be used to determine the optical thickness of the atmosphere. The optical thickness is the most important parameter for atmospheric correction of remote sensor data.

Dr. Robert E. Turner was the principal investigator for this project. He performed the mathematical analysis and devised the computer program for the simulation studes. He would like to acknowledge the assistance of Mr. Joseph L. Manning who ran the computer program and helped in the plotting of graphs.

In the course of this work informative discussions were held with Professor James Smith of Colorado State University. We also acknowledge the direction provided by Mr. Charles W. Aitken of ORI, Inc.

TABLE OF CONTENTS

1
INTRODUCTION

In the last ten years an enormous data base of information has been created on the spectral radiation of the Earth's surface. In early years, most of the data were collected by using multispectral sensors aboard aircraft, whereas in the later years most of the data were acquired with sensors on spacecraft such as Skylab and Landsat. Of particular concern to many users of the data is the image degradation or the probability of misclassification which arises from atmospheric effects.

Earth's atmosphere contains a semi-permanent suspension of particulates called an aerosol. The aerosol manifests itself in the form of light haze, industrial air pollution, heavy haze, fogs, and clouds. It is this aerosol component which is the important factor in the correction of remote sensor data for atmospheric effects.

In this report we shall be concerned with particular radiometric satellite techniques which can be used with the proposed MRS sensor to account for atmospheric effects in remote sensing. We describe a computer simulation of the Multispectral Resource Sampler (MRS) sensor for specific targets. In addition, we describe algorithms which can be used to determine the spectral optical thickness of the atmosphere provided the reflectances of "standard" targets are known.

2
REMOTE SENSING OF THE EARTH's SURFACE

Sensors on satellites in Earth orbit are usually designed to detect electromagnetic radiation in a number of spectral bands specifically chosen so as to maximize the signal to background ratio for objects of interest. The ultraviolet region generally is not used because atmospheric gases absorb most of the radiation at those wavelengths. Likewise, we must take special care in the infrared region because there are strongly absorbing gases in the infrared. In addition, the greatest amount of solar-reflected energy is in the visible part of the spectrum. For these reasons the near ultraviolet, visible and near infrared regions are chosen for radiometric sensors. For the analysis of atmospheric effects using the MRS sensor the atmospheric working group decided on the spectral bands; 360-400 nm; 490-510 nm; 630-690 nm; and 930-950 nm.

In this section we shall be concerned with the description of the natural radiation field in the atmosphere and how it can be used to account for and to determine the optical properties of the atmosphere.

2.1 RADIATIVE TRANSFER THEORY

Radiation enters the atmosphere and is scattered and absorbed by gases and particulates. If one has a description of the optical properties of the atmospheric gases and particulates in terms of altitude over a particular target area, and a knowledge of the terrain, then, in principle, it should be possible to calculate the spectral radiation field. A complete description does not exist however, and even an approximate description of the optical properties of the atmosphere is difficult to obtain, at least for a large portion of the Earth's surface. Nevertheless, if we have some information regarding the reflectance properties of specific targets, than we can determine a quantity called the

spectral optical thickness of the atmosphere. The primary reason that we are now able to accomplish this task is that the MRS sensor can "lock onto" a target and observe that target as the nadir view angle changes. This was not possible with previous satellite sensors.

2.1.1 INTERACTION PROCESSES

As radiation enters a scattering-absorbing medium there are several processes or interaction mechanisms to consider in a mathematical description of the radiation field. These all illustrated for a volume element in Figure 1. Within the context of radiometry the first process is that of no interaction (zero gain and zero loss) for radiation streaming into a sensor. The second process is the loss of radiation by absorption. Third, we have radiation which is scattered out of the field of view, resulting in a loss. Fourth, there is a gain of radiation which results from the scattering of radiation into the field of view. Fifth, radiation can be emitted by sources in the field of view.

The loss mechanisms attenuate the radiation between source and sensor and this can be expressed as the transmittance along a path s, i.e.:

$$T(\lambda,s) = \exp\left\{-\int_0^s \kappa(\lambda,s')ds'\right\} \qquad (1)$$

Where $\kappa(\lambda,s')$ is the volume extinction coefficient at wavelength λ and point s along the path.

The gain mechanisms of scattering and emission give rise to what is referred to as the path radiance, $L_p(\lambda,s,\hat{\Omega})$, a quantity which is a function of wavelength λ, position s, and direction $\hat{\Omega}$.

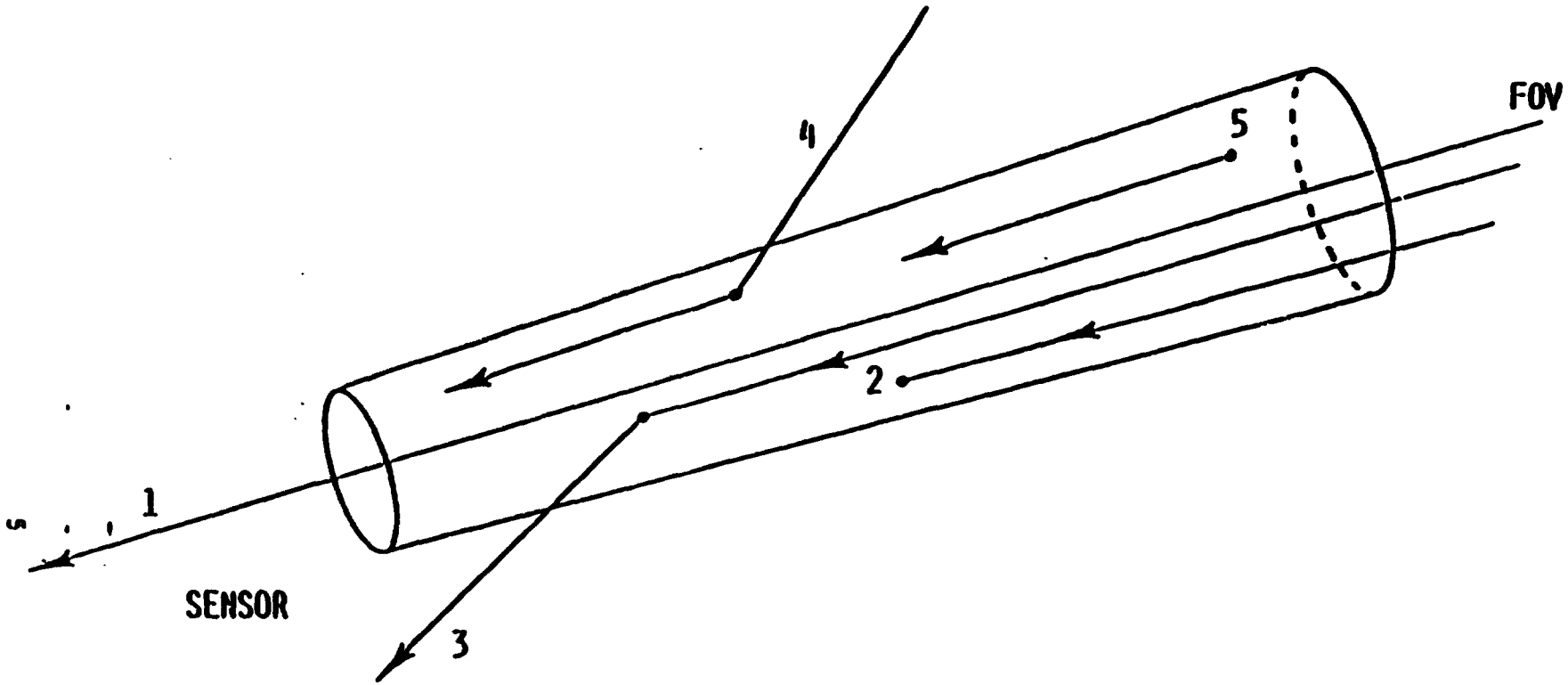

FIGURE 1 INTERACTION MECHANISMS

1. NON-INTERACTING RADIATION (NO GAIN, NO LOSS)
2. ABSORBED RADIATION (LOSS)
3. SCATTERED RADIATION (LOSS)
4. SCATTERED RADIATION (GAIN)
5. EMITTED RADIATION (GAIN)

For the purposes of this investigation we do not need to be concerned with the details of the optical properties of the atmospheric constituents. We only need to understand the general definitions. An important optical quantity is the spectral optical thickness, defined as:

$$\tau(\lambda,\theta) = \sec\theta \int_0^{\infty} \kappa(\lambda,z')\, dz' \qquad (2)$$

where z' is the vertical distance from the Earth's surface, and θ is the zenith angle. It should be noted that optical thickness is usually defined as $\tau_0(\lambda,0)$, along a vertical path instead of a slant path. For this investigation however, with its special emphasis on view angle we will use the definition of Equation 2.

2.1.2 REMOTE SENSING EQUATION

The spectral raidance is the amount of radiation flowing in a specific direction per unit area per unit time per unit solid angle per unit spectral interval. In the model used in this report we use units of milliwatts per square centimeter per steradian per micrometer of wavelength. Let the spectral radiance at the sensor be $L(\lambda,0,\hat{\Omega})$ where 0 denotes the optical depth τ which is measured from the top of the atmosphere downwards. Let $L(\lambda,\tau_0,\hat{\Omega})$ be the spectral radiance of the target <u>at</u> the target, i.e. at $\tau = \tau_0$. The radiance at the sensor can then be written as

$$L(\lambda,0,\hat{\Omega}) = L_0(\lambda,\tau_0,\hat{\Omega})T(\lambda,\tau_0,\hat{\Omega}) + L_p(\lambda,\tau_0,\hat{\Omega}). \qquad (3)$$

Eq. 3 can be called the remote sensing equation. If the path radiance $L_p(\lambda,\tau,\hat{\Omega})$ and the transmittance $T(\lambda,\tau_0,\hat{\Omega})$ can be measured or calculated then a measurement of the sensor radiance $L(\lambda,0,\hat{\Omega})$ yields the target radiance $L_0(\lambda,\tau_0,\hat{\Omega})$. It should be noted however, that the surface radiance is <u>not</u> independent of the atmosphere because it depends upon the radiance incident upon the target and that is a function of the sky radiance. An illustration of the MRS geometry is depicted in Figure 2 for three nadir view angles and three azimuth angles.

2.1.3 EQUATION OF TRANSFER

If we consider the gain and loss mechanisms illustrated in Figure 1, we can write an equation for the transfer of radiation. The time-independent, three dimensional radiative-transfer equation [1] is:

$$\hat{\Omega} \cdot \nabla L(\lambda,\vec{r},\hat{\Omega}) = -\kappa(\lambda,\vec{r})L(\lambda,\vec{r},\hat{\Omega}) + \frac{\beta(\lambda,\vec{r})}{4\pi}\int_{4\pi} p(\vec{r},\hat{\Omega}\cdot\hat{\Omega}')L(\lambda,\vec{r},\hat{\Omega}')d\hat{\Omega}' + \alpha(\lambda,\vec{r})B(\lambda,\vec{r}) + S(\lambda,\vec{r},\hat{\Omega}). \quad (4)$$

where κ,α, and β are the volume extinction, volume absorption, and volume scattering coefficients respectively, and p is the scattering phase function. The left hand side of the equation defines the spatial rate of change in the radiance at point $\vec{r}(x,y,z)$ in the medium for radiation in direction $\hat{\Omega}$. The first term on the right hand side defines the loss due to scattering and absorption; the second term describes the gain due to scattering into the field of view; the third term describes the gain due to thermal emission; and the last term describes some additional source.

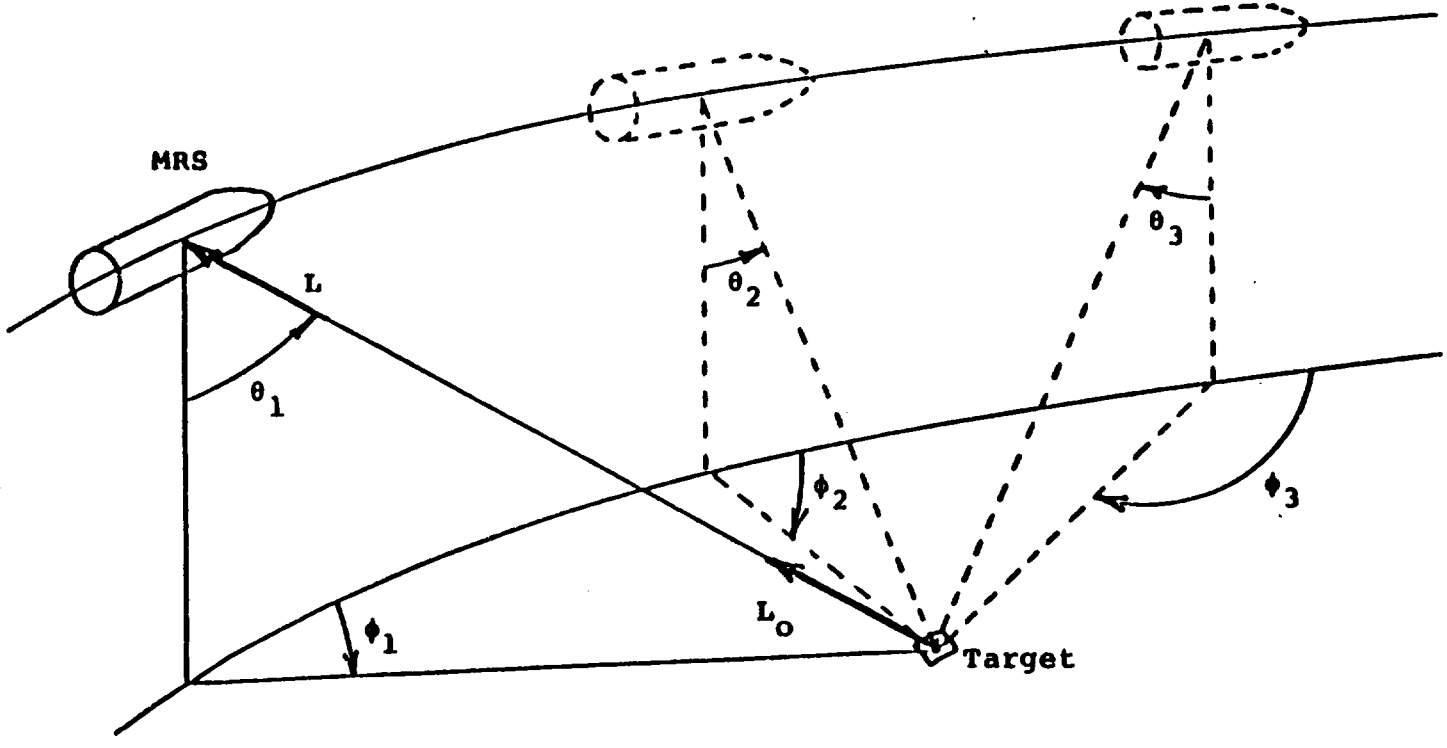

FIGURE 2. VARIATION OF NADIR VIEW ANGLE FOR THE MRS FOR A SPECIFIC "TARGET"

The general three-dimensional problem is a very difficult one to solve. We shall consider the simpler one-dimensional problem in which there is a variation in the vertical direction only. The corresponding one-dimensional equation [1] (neglecting source S) is:

$$\mu \frac{dL}{d\tau} = L(\tau,\mu,\phi) - \frac{\omega_0(\tau)}{4\pi} \int_0^{2\pi}\int_{-1}^{1} p(\tau,\mu,\phi,\mu',\phi') L(\tau,\mu',\phi') d\mu' d\phi'$$

$$- \left(1 - \omega_0(\tau)\right) B(\tau), \qquad (5)$$

where $\mu = \cos\theta$ and $\omega_0(\tau)$ is called the single-scattering albedo. For the MRS bands we can neglect the last term in Equation 5 because thermal emission is negligible.

2.1.4 BOUNDARY CONDITIONS

The complete radiation field in the atmosphere is determined if one solves Eq. 5 subject to the following boundary conditions:

$$L(0,\mu,\phi) = \mu E_0 \, \delta(\mu + \mu_0)\delta(\phi - \phi_0) \qquad (6)$$

and

$$L(\tau_0,\mu,\phi) = \mu_0 E_0 \, \rho(\mu,\phi, -\mu_0,\phi_0) e^{-\tau_0/\mu_0}$$

$$+ \int_0^{2\pi}\int_0^{1} \mu' \rho(\mu,\phi,\mu',\phi') L_s(\tau_0,\mu',\phi') d\mu' d\phi' \qquad (7)$$

where E_0 is the extraterrestrial solar irradiance, θ_0 is the solar zenith angle and ϕ_0 is the solar azimuth angle. The function $\rho(\mu,\phi,\mu',\phi')$ is the general, bi-directional reflectance of the surface and $L_s(\tau_0,\mu',\phi')$ is the sky radiance. The radiance $L(\tau_0,\mu,\phi)$ is the same as the radiance $L_0(\lambda,\tau_0,\hat{\Omega})$ in Eq. 3 for a specific target. If one knows the bi-directional reflectance for the surface, then the surface radiance can be calculated using Eq. 7 provided the sky radiance is known.

For a very clear sky with little haze the integral term in Eq. 7 is small compared to the direct solar reflectance term. On the other hand, for a hazy or overcast sky the first term is negligible. In another section we will use Eq. 7 to analyze the atmosphere using MRS correction algorithms.

For a perfectly diffuse or Lambertian surface, Eq. 7 becomes

$$L(\tau_0,\mu,\phi) = \frac{\bar{\rho}}{\pi} E(\tau_0) \tag{8}$$

where $\bar{\rho}$ is the surface albedo which is independent of direction and $E(\tau_0)$ is the total (solar plus sky) irradiance.

2.2 A RADIATION MODEL

A number of computational methods have been developed over the last ten years which are used to calculate the spectral radiance in the atmosphere. In almost all cases there is usually an excessive amount of computer time for the computation because of the large number of scatterings to be represented. Chandrasekhar [1] was one of the first investigators who found an exact solution to the radiation

transfer problem with multiple scattering in a molecular (Rayleigh) atmosphere bounded by perfectly diffuse (Lambertian) surfaces. Today, many other computational techniques are used to calculate the radiation field. A brief description of most of the current methods is given in a State-of-the-Art report [2]. One of these methods, developed by Turner [3,4,5,6,7] makes use of an approximation in the radiation field to arrive at a closed-form solution for the spectral radiance. The input and output quantities for this radiative-transfer model are illustrated in Figure 3. Using the results of Coulson et al. [8] which were computations based upon Chandrasekhar's analysis, we compared the calculated radiances with those based upon the Turner radiative-transfer model. These comparisons are illustrated in Figure 4,5, and 6 for various sun angles and surface albedos. Although the atmosphere is a pure molecular one in which the horizontal visual range is 336 km, the agreement is very good. We have also compared the model with experimental data on sky radiance by Ivanov [9] for clear skies. These comparisons are depicted in Figures 7,8, and 9 for different sun angles and again, the agreement is very good.

It is interesting to look at a polar plot of the radiance as seen by a ground observer (sky radiance) and the total radiance (surface plus path) as seen by an observer in a satellite. Using the radiative-transfer model Turner [10] calculated and plotted these radiances as a function of zenith and nadir view angle for various surface albedos and atmospheric optical thicknesses. Examples of the radiances are illustrated in Figures 10 and 11 for Rayleigh scattering. The only difference between the two plots is the optical thickness. In Figure 11 the optical thickness is ten times that in Figure 10 and the sky radiance is much greater. If

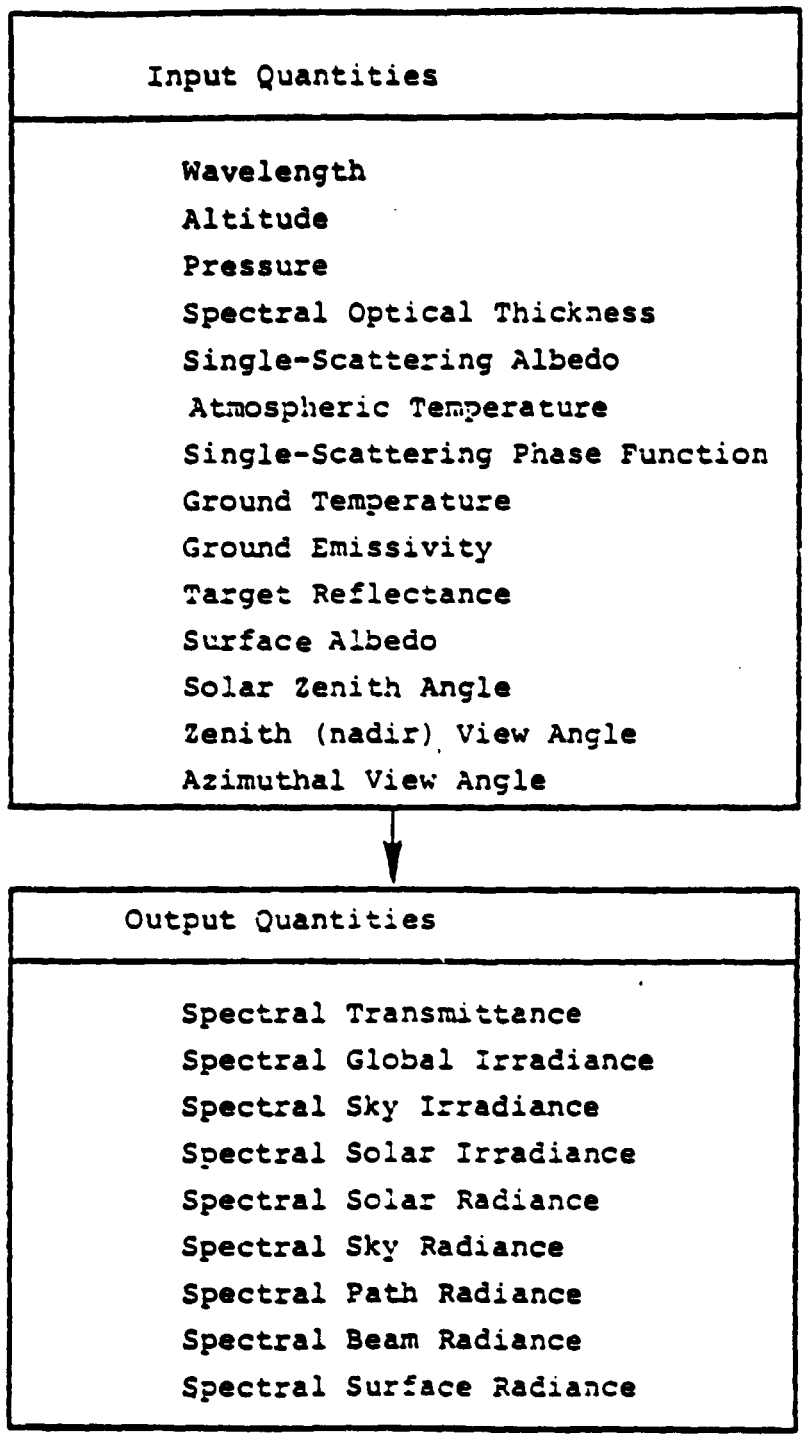

Figure 3 - Atmospheric Radiative Transfer Model Developed by R.E. Turner.

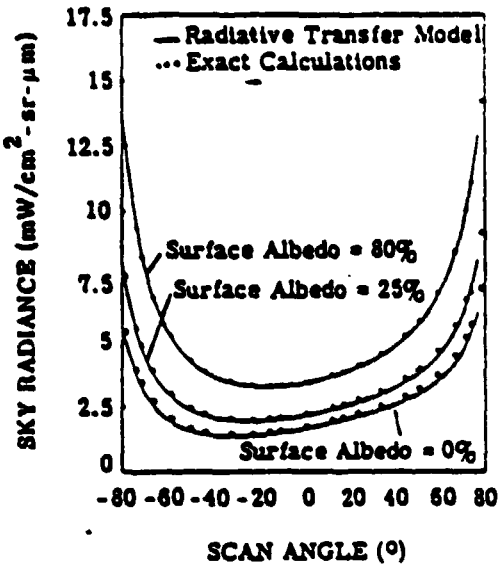

FIGURE 4. DEPENDENCE OF SKY RADIANCE ON SCAN ANGLE (IN THE SOLAR PLANE); SOLAR ZENITH ANGLE = 36.9°. Visual range = 336 km; wavelength = 0.546 μm.

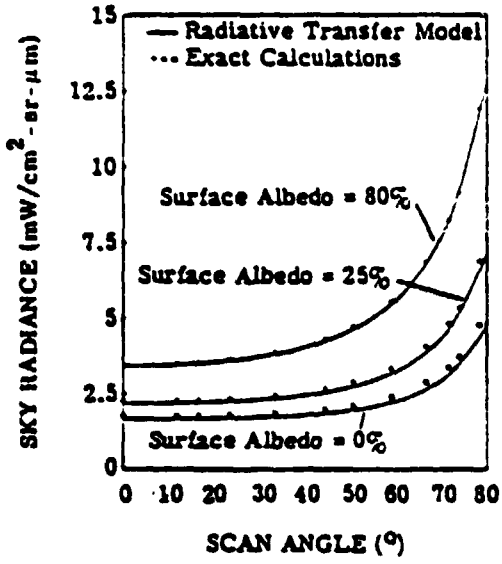

FIGURE 5. DEPENDENCE OF SKY RADIANCE ON SCAN ANGLE (PERPENDICULAR TO THE SOLAR PLANE); SOLAR ZENITH ANGLE = 36.9°. Visual range = 336 km; wavelength = 0.546 μm.

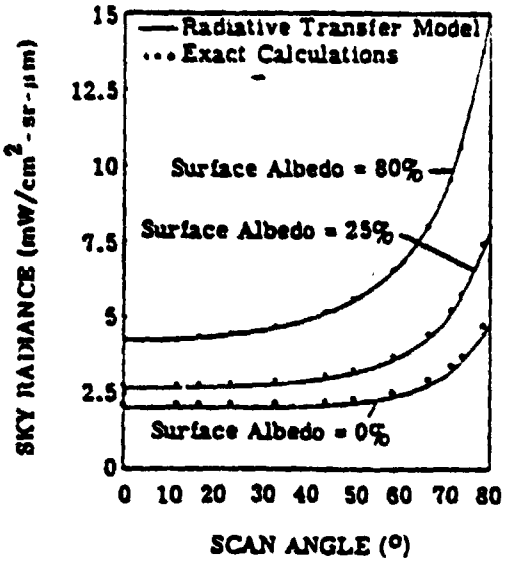

FIGURE 6. DEPENDENCE OF SKY RADIANCE ON SCAN ANGLE (IN THE SOLAR PLANE); SOLAR ZENITH ANGLE = 0°. Visual range = 336 km; wavelength = 0.546 μm.

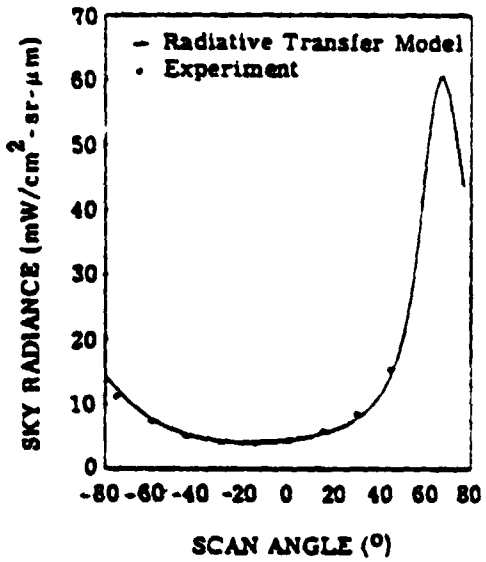

FIGURE 7. DEPENDENCE OF SKY RADIANCE ON SCAN ANGLE (IN THE SOLAR PLANE); SOLAR ZENITH ANGLE = 65.8°. Visual range = 269 km; wavelength = 0.404 μm; surface albedo = 45%

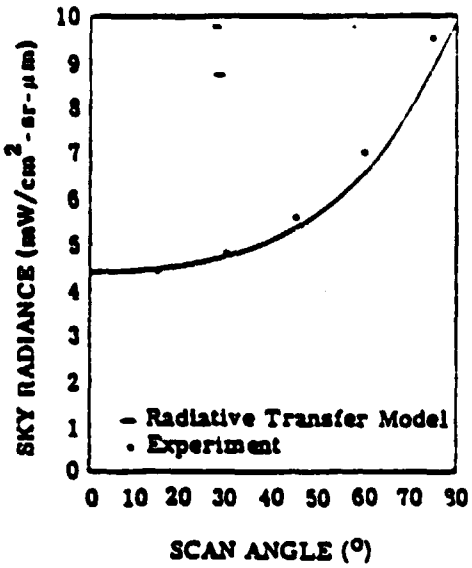

FIGURE 8. DEPENDENCE OF SKY RADIANCE ON SCAN ANGLE (PERPENDICULAR TO THE SOLAR PLANE); SOLAR ZENITH ANGLE = 65.8°. Visual range = 269 km; wavelength = 0.404 μm; surface albedo = 45%

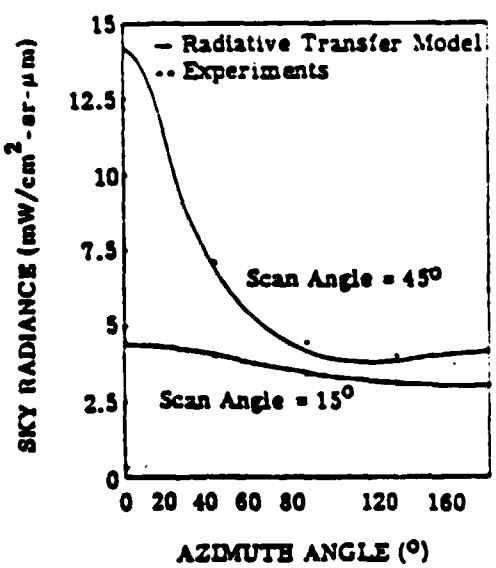

FIGURE 9. DEPENDENCE OF SKY RADIANCE ON AZIMUTH ANGLE. Visual range = 261 km; wavelength = 0.447 μm; surface albedo = 16%; solar zenith angle = 65.7°.

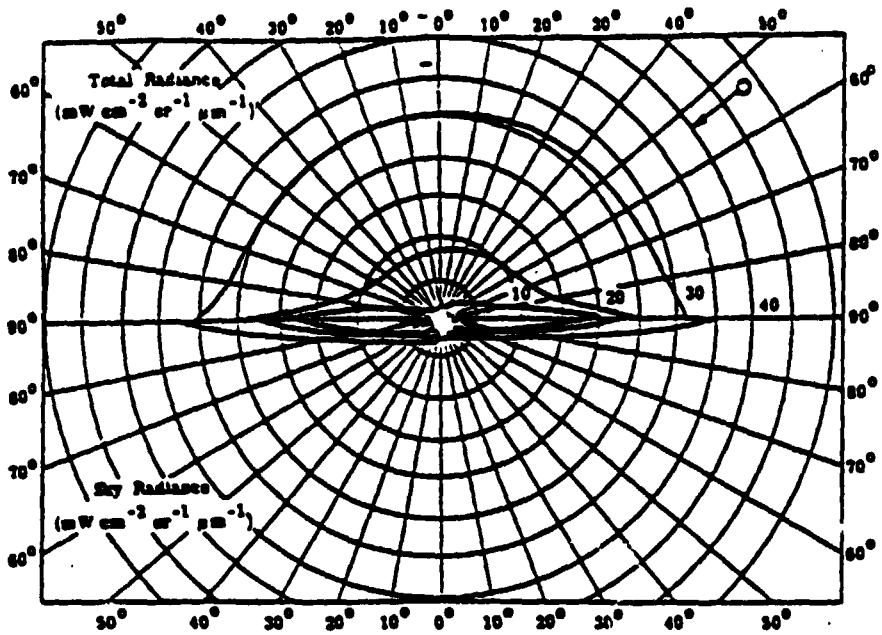

Fig. 10. Total radiance and sky radiance as a function of view angle in the solar plane for a Rayleigh atmosphere and three reflectances. θ_o is 53°8'; τ_o is 0.1; λ is 0.55 μm; the day is June 21; and ρ is 0.0, 0.25, and 0.80.

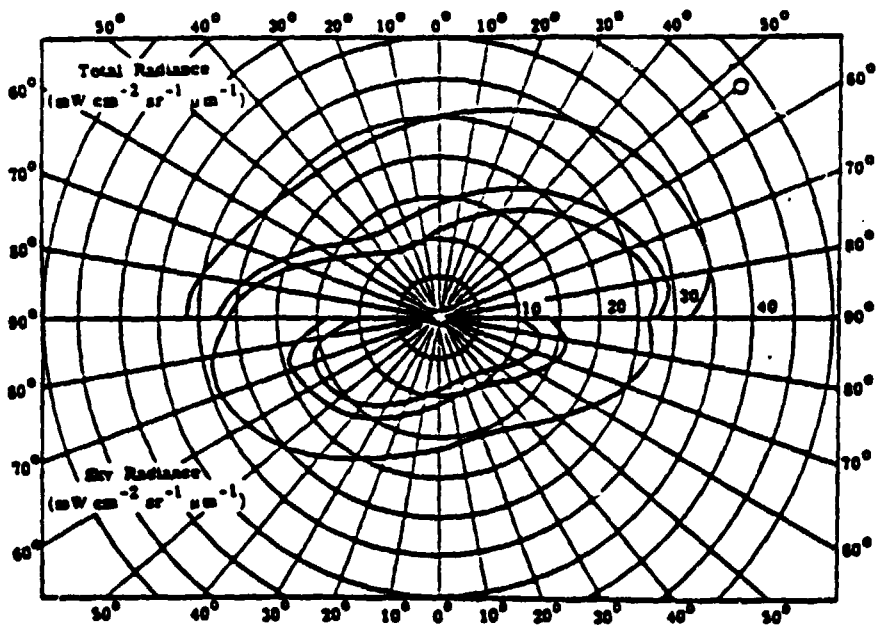

Fig. 11. Total radiance and sky radiance as a function of view angle in the solar plane for a Rayleigh atmosphere and three reflectances. θ_o is 53°8'; τ_o is 1.0; λ is 0.55 μm; the day is June 21; and ρ is 0.0, 0.25, and 0.80.

one adds an aerosol component to the atmosphere the scattering is predominantly in the forward direction. This effect is noticed in Figure 12 in which the total optical thickness is 0.10 and the Rayleigh Optical thickness is 0.098. If the aerosol component is increased so that the total optical thickness is 0.2, characteristic of an atmosphere with a horizontal visual range of about 250 km, then the radiance is that depicted in Figure 13. Here the strong forward scattering is evident as well as the typical increase in the backward direction. If we increase the optical thickness to a value of 1, representative of a horizontal visual range of about 44 km, then the solar aureole is very pronounced as is illustrated in Figure 14. It should be noted that the scale has been changed to accommodate the larger radiance value in the forward scattering direction. All of the illustrations are for Lambertian targets and backgrounds and for atmospheres which are uniform in the horizontal direction. In another section we will deal with non-Lambertian targets and inhomogeneous atmospheres.

It is also of interest to observe the path radiance and the sky radiance as a function of time (or sun angle) and the nadir or zenith view angle. These radiances are depicted in Figures 15 and 16 for a hazy atmosphere. The back-scattering peak is clearly evident in the path radiance and the solar aureole is obvious in the sky radiance. The effect of surface albedo and visual range on the radiances is illustrated in Figures 17 and 18. The multiple scattering of radiation is much greater for the shorter wavelengths and low visual ranges than for longer wavelengths and clear skies.

In conclusion, the present radiative-transfer model seems to be in agreement with the more detailed, exact mathematical methods and also with experimental data. We will make use of calculations based upon this model for the MRS simulation.

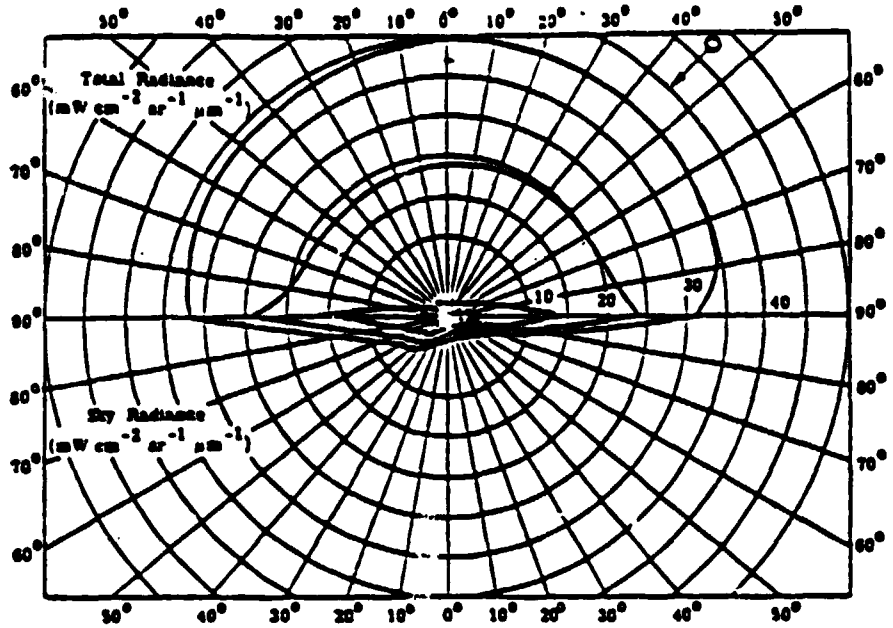

Fig. 12. Total radiance and sky radiance as a function of view angle in the solar plane for three reflectances. θ_0 is 45°; τ_0 is 0.10; λ is 0.55 μm; the day is June 21; and ρ is 0.0, 0.5, and 0.9.

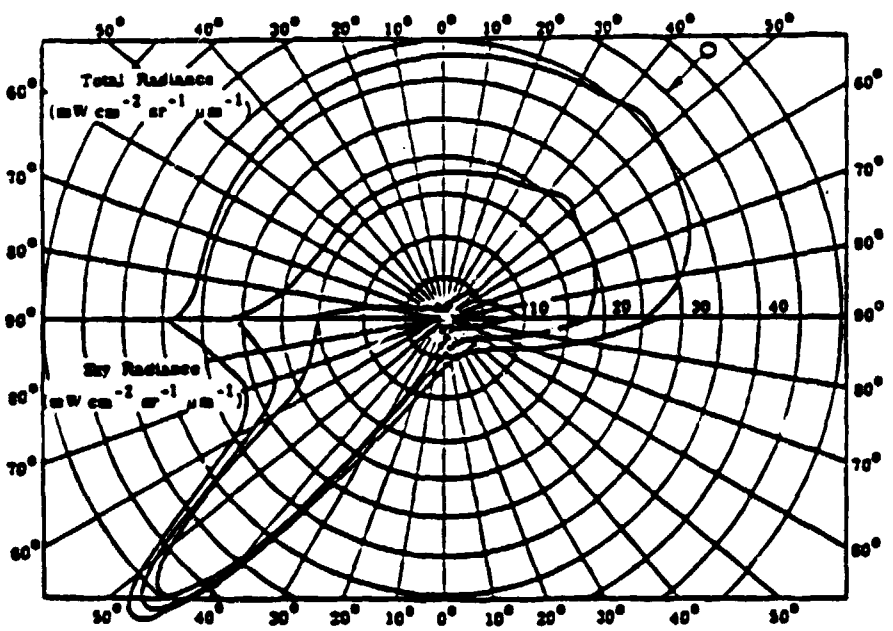

Fig. 13. Total radiance and sky radiance as a function of view angle in the solar plane for three reflectances. θ_0 is 45°; τ_0 is 0.2; λ is 0.55 μm; the day is June 21; and ρ is 0.0, 0.5, and 0.9.

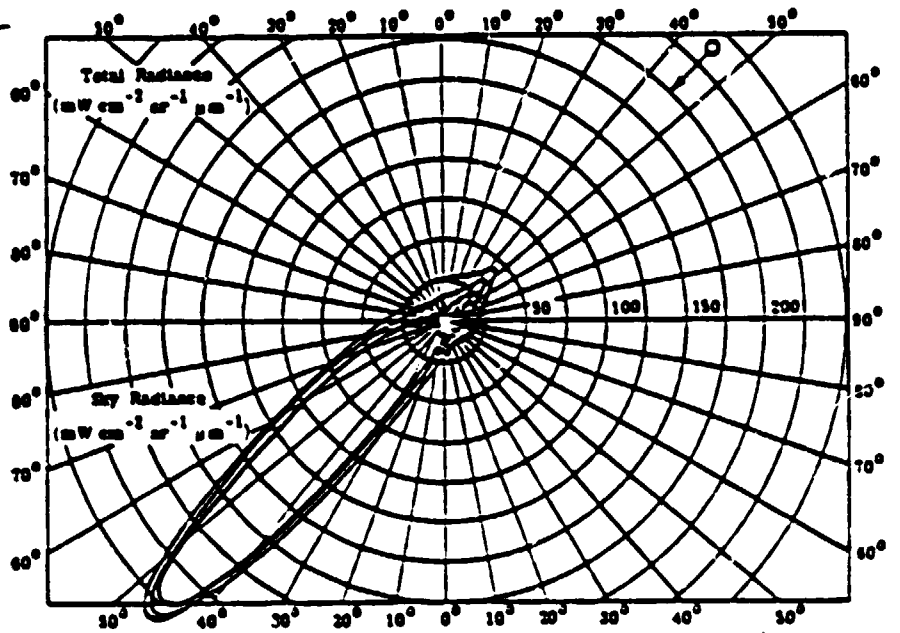

Fig. 14. Total radiance and sky radiance as a function of view angle in the solar plane for three reflectances. θ_o is 45°; r_o is 1.0; λ is 0.55 μm; the day is June 21 and ρ is 0.0, 0.5, and 0.9.

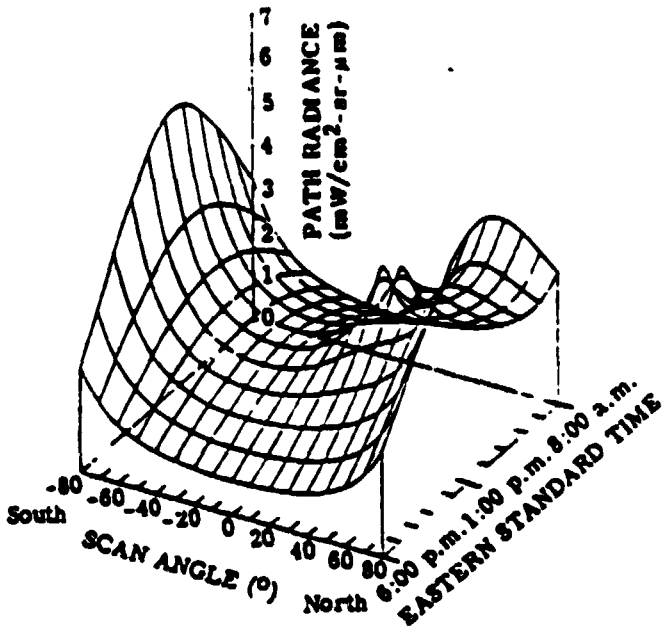

FIGURE 15. DEPENDENCE OF PATH RADIANCE ON TIME AND SCAN ANGLE. Southeastern Michigan, 1 September 1971. Wavelength = 0.55 μm; altitude = 1 km; visual range = 8 km; surface albedo for green vegetation.

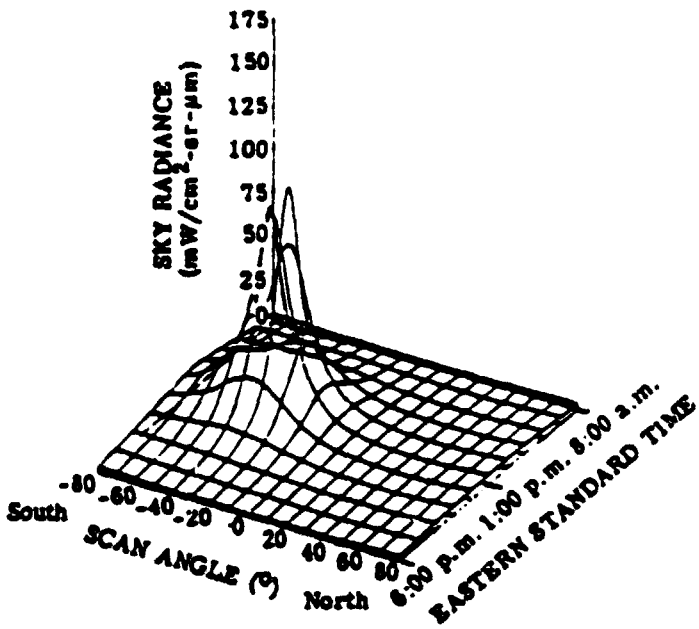

FIGURE 16. DEPENDENCE OF SKY RADIANCE ON TIME AND SCAN ANGLE. Southeastern Michigan, 1 September 1971. Altitude = 0 km; wavelength = 0.55 μm; visual range = 8 km; surface albedo for green vegetation.

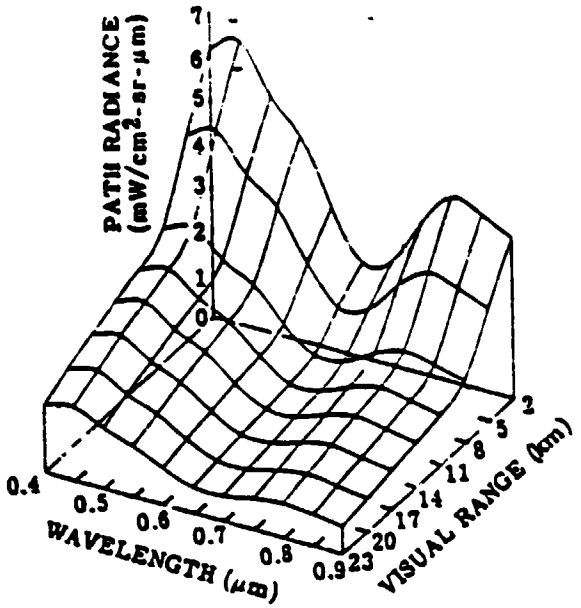

FIGURE 17. DEPENDENCE OF PATH RADIANCE ON VISUAL RANGE AND WAVELENGTH. Solar zenith angle = 30°; scan angle = 0°; azimuthal angle = 0° (in the plane of the sun); altitude = 1 km; surface albedo for green vegetation.

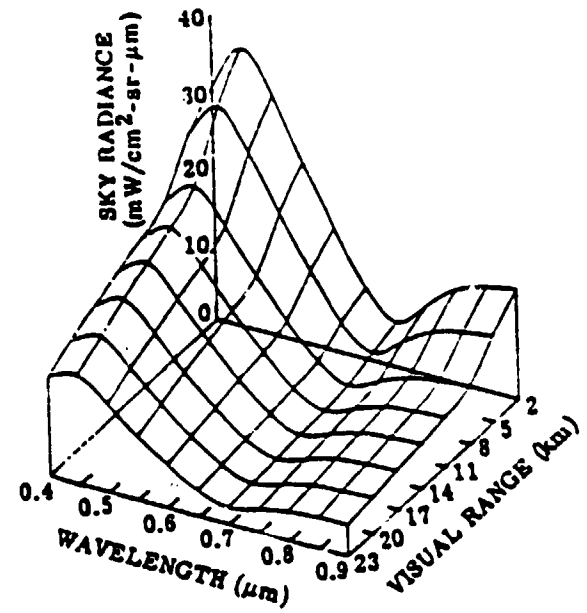

FIGURE 18. DEPENDENCE OF SKY RADIANCE ON VISUAL RANGE AND WAVELENGTH. Solar zenith angle = 30°; scan angle = 0°; altitude = 0 km; azimuthal angle = 0° (in the plane of the sun); surface albedo for green vegetation.

3
THE MULTISPECTRAL RESOURCE SAMPLER

The Multispectral Resource Sampler (MRS) is an experimental pushbroom scan sensor being developed by NASA for Earth orbiting spacecraft flight in the mid-1980's. It's major advantage over existing systems is it's capability to point at and fix on a particular object on the Earth's surface as the spacecraft move in an orbit. In this section we will use the radiative-transfer model to simulate the spectral radiances at the sensor for various angles, wavelengths, atmospheres, and targets.

3.1 MRS SIMULATION

A technical publication by Schnetzler and Thompson [11] described the Multispectral Resource Sampler and its detailed spectral characteristics. The MRS sensor characteristics are listed in Table 1. The spectral bands to be used in the MRS depend upon the properties of the materials being investigated. These are illustrated in Figure 19. For the investigation of the atmospheric properties, one needs to know the atmospheric optical thickness in order to calculate the transmittance and path radiance. In this section we will use various optical thicknesses to calculate the spectral radiances at the sensor. The optical properties of the atmosphere, the angles to be considered, and the spectral reflectance of the vegetative background are given in Tables 2 and 3. The nadir view angles are those which correspond to equal increments in secant θ, i.e. 1.0, 1.1, 1.2, ... The optical thicknesses are those which correspond to the simple Elterman [12] exponential haze model characterized by a surface horizontal visual range. Thus, we will consider V = 2 km (heavy haze), V = 13 km (moderate haze), and V = 40 km (light haze). The single-scattering phase functions and the

TABLE 1

MRS Sensor Characteristics

Spectral Range:	0.36 μm to 1.0 μm
Spectral Bands:	4 arrays, each with 2000 detectors 5 selectable filters/array Bandwidths $\geq$ 20 nm Polarization filters
Spatial Resolution:	15 meters max
Swath Width/Modes:	15 km at 15 m (4 bands) 30 km at 15 m (2 bands) at 15 m (4 bands, 50% sampling) at 30 m (4 bands)
Radiometric Sensitivity:	Approximately 0.5% $NE\Delta\rho$ (8 bit)
Data Rate:	15 mega bits/sec.
Pointability:	2 axes $+ 40^{o}$ across track $+ 55^{o}$ along track
Speed of Pointing:	30^{o}/sec across track 5^{o}/sec along track

MRS SPECTRAL BANDS

		ARRAY NO.				REMARKS
		1	2	3	4	
FILTER POSITION	1	450-520 TM 1	520-600 TM 2	630-690 TM 3	760-900 TM 4	THEMATIC MAPPER BANDS
	2	540-560	670-690	710-730	780-800	VEGETATION
	3	840-860	880-900	730-750	400-420	GEOL. VEG
	4	360-400	TM 3 VERT.	930-950	490-510	ATMOS. LAND USE POLAR.
	5	TM 4 VERT.	TM 4 HORZ.	TM 2 HORZ.	TM 3 HORZ.	POLARIZE

UNITS IN NANOMETERS

Figure 19. MRS Spectral Bands

TABLE 2. ANGLES FOR MRS SIMULATION

Solar Zenith Angle θ_0 = 30°, 60°
Azimuth Angle ϕ = 0°, 90°, 180°
Nadir View Angle θ = 0°, 24.62°, 33.56°, 39.72°, 44.42°, 48.19°, 51.32°, 53.97°, 56.25°, 58.24°, 60.00°.

TABLE 3. OPTICAL PROPERTIES FOR MRS SIMULATION

λ (μm)	0.380	0.500	0.660	0.940
τ_0 (V = 2)	2.881	1.968	1.410	1.000
τ_0 (V = 13)	1.030	0.587	0.390	0.250
τ_0 (V = 40)	0.720	0.370	0.222	0.132

λ - Wavelength (μm)

τ_0 - Optical Thickness with Surface Visual Range V *

$\bar{\rho}$ - Albedo (Diffuse Reflectance) of Vegetative Background

*Deirmendjian's Haze Model L was used for the aerosol size distribution with a particulate refractive index of m = 1.5 - 0.01 i and a single-scattering albedo of 0.97.

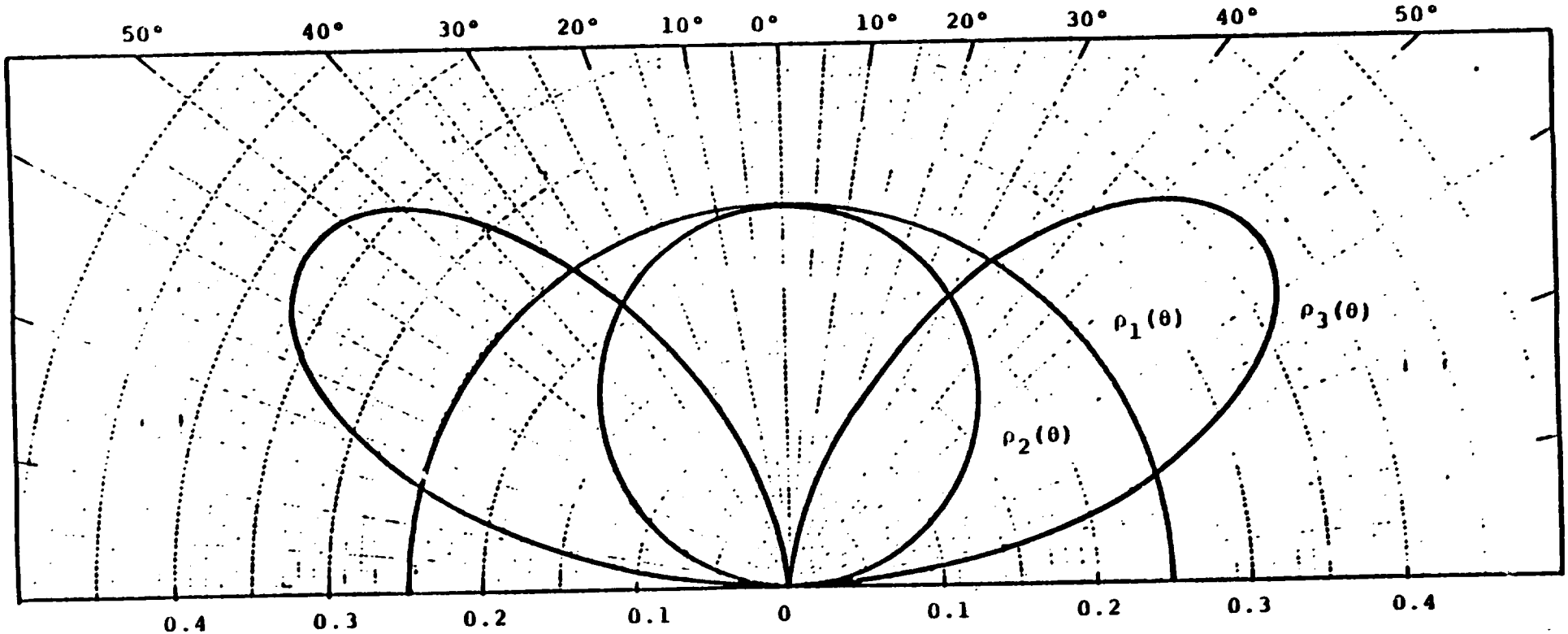

FIGURE 20. BI-DIRECTIONAL REFLECTANCE DISTRIBUTION FUNCTIONS IN ANY AZIMUTHAL PLANE

$$\rho_1(\theta) = 0.25$$
$$\rho_2(\theta) = 0.25 \cos \theta$$
$$\rho_3(\theta) = \cos \theta \sin^2 \theta$$

single-scattering albedo used in the calculation of radiances are for an index of refraction m = 1.5 - 0.01 i, that is, for a slightly absorbing atmosphere. The background surface albedo is that for green vegetation.

3.1.1 TARGET REFLECTANCES

The general radiance at the surface in the upward direction is given by Eq. 7. If the bi-directional reflectance distribution function $\rho(\mu,\phi,\mu',\phi')$ were known then one could calculate the surface radiance. Rather than perform this tedious numerical analysis we will consider the surface radiance to have simple radiation patterns. We will use the following surface reflectances in our MRS simulation:

$$\rho_1(\theta) = 0.25 \tag{9}$$

$$\rho_2(\theta) = 0.25 \cos\theta \tag{10}$$

$$\rho_3(\theta) = \cos\theta \sin^2\theta \tag{11}$$

The functions are represented graphically in Figure 20. The first function, $\rho_1(\theta)$ is a diffuse (Lambertian) surface and the other two represent hypothetical surfaces. All functions have azimuthal symmetry.

3.1.2 MRS SENSOR RADIANCES

Using the three reflectance functions above and the radiative-transfer model we calculated the sensor radiance as given by Eq. 3. In Figure 21 we plot the radiance at a wavelength of 0.380 μm vs. the secant of the nadir view angle for the Lambertian target. There is a large peak in the radiance in the anti-solar direction for the extremely hazy

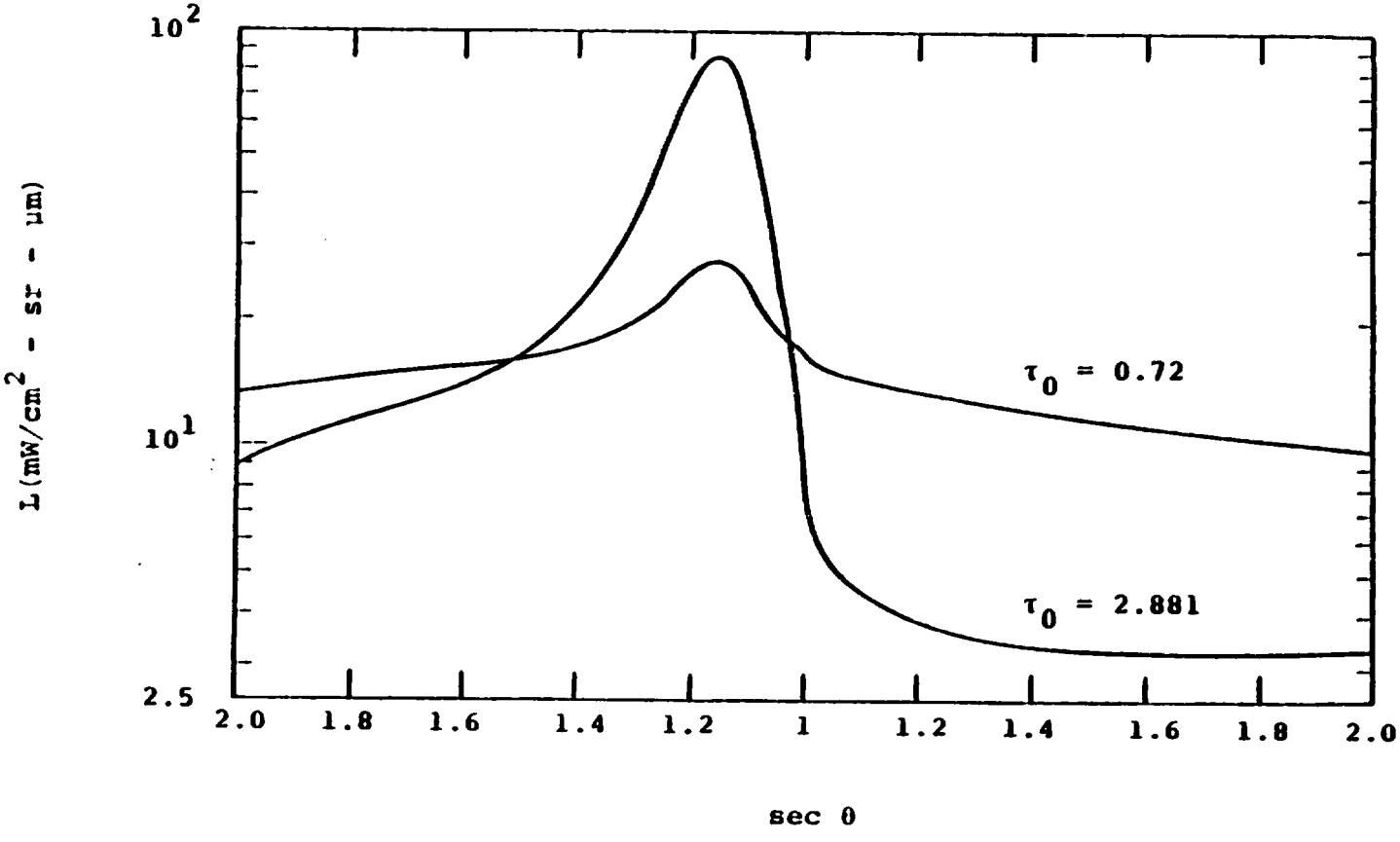

FIGURE 21. RADIANCE AT 0.380 μm vs. THE SECANT OF THE NADIR VIEW ANGLE IN THE SOLAR PLANE FOR A WHITE DIFFUSE TARGET AND A VEGETATIVE BACKGROUND. SOLAR ZENITH ANGLE = 30°.

(V = 2 km) atmosphere and a smaller peak for the light haze (V = 40 km). It should be noted that the target reflectance for the diffuse target is one and not 0.25 as in Figure 20. The second target was used for the same situation and the resulting radiances are plotted in Figure 22. As expected, the radiance decreases more rapidly with increasing angle because of the cosine surface distribution. The third reflectance function was used and its corresponding radiances are illustrated in Figure 23. Here it should be noted that the path radiance is for sec θ = 1 because of the value of zero for the reflectance function when θ = 0°.

There should be a large change in radiance values for different wavelengths. This is illustrated in Figure 24 for the diffuse target and in Figure 25 for the third target. As expected the backscattered radiation at the anti-solar angle is much greater for the short wavelengths than for the long wavelengths. For the large angles, however, the change in the transmittance is greater than the change in path radiance and the opposite relationship is found.

All of these curves can change radically if the sun angle is different. This solar angle effect is illustrated in Figure 26, 27, and 28 for the three targets. As expected, the maximum is attained for the backscattering direction for the anti-solar angle, in this case when sec θ = 2.

Finally, we consider the case in which the orbit of the spacecraft is normal to the solar plane. As the sensor passes over the target the radiance distribution with angle should be symmetric for a horizontally homogeneous atmosphere. This effect is illustrated in Figures 29, 30, and 31.

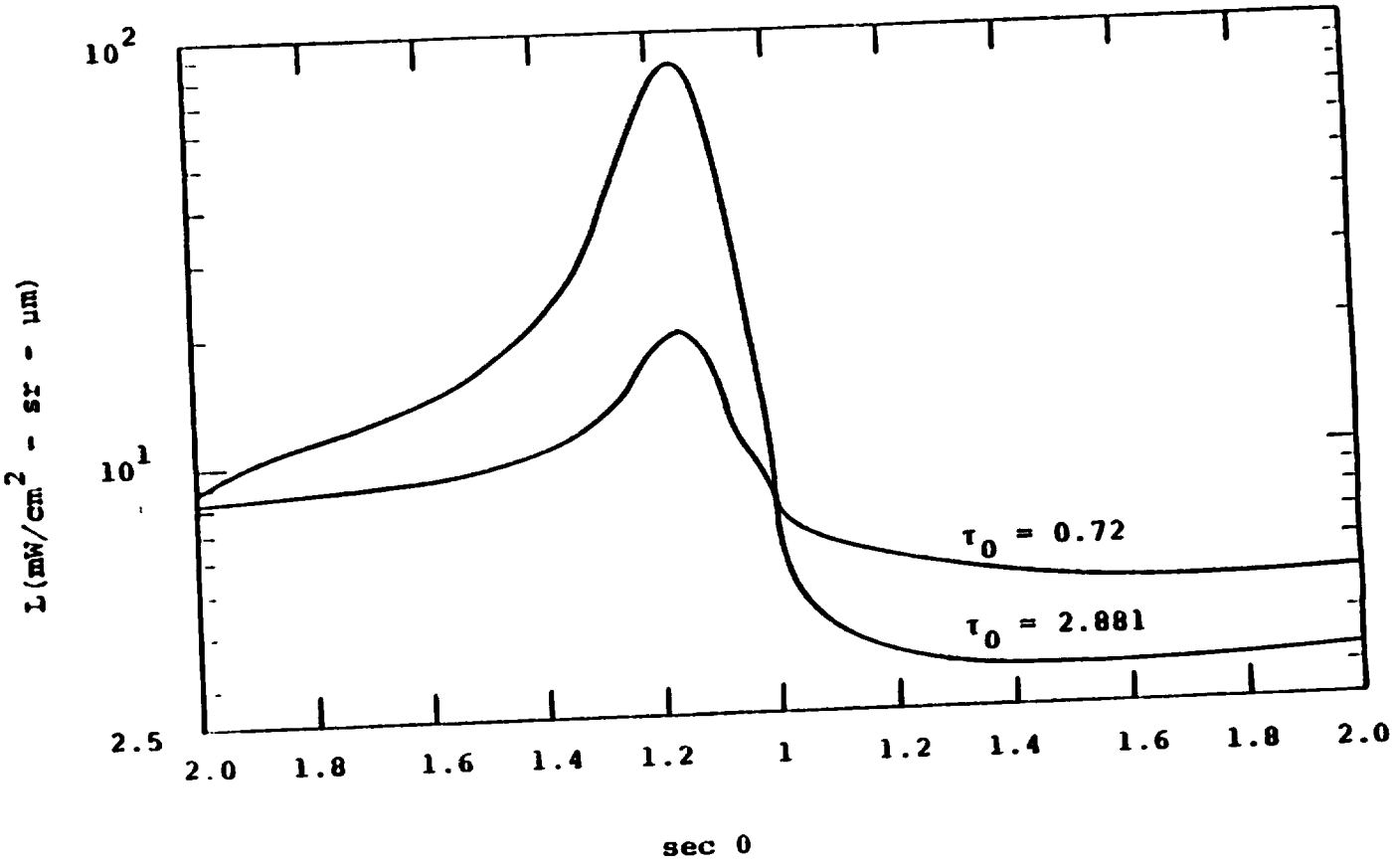

FIGURE 22. RADIANCE AT 0.380 μm vs. THE SECANT OF THE NADIR VIEW ANGLE IN THE SOLAR PLANE FOR A "COSINE" TARGET AND A VEGETATIVE BACKGROUND. SOLAR ZENITH ANGLE = 30°.

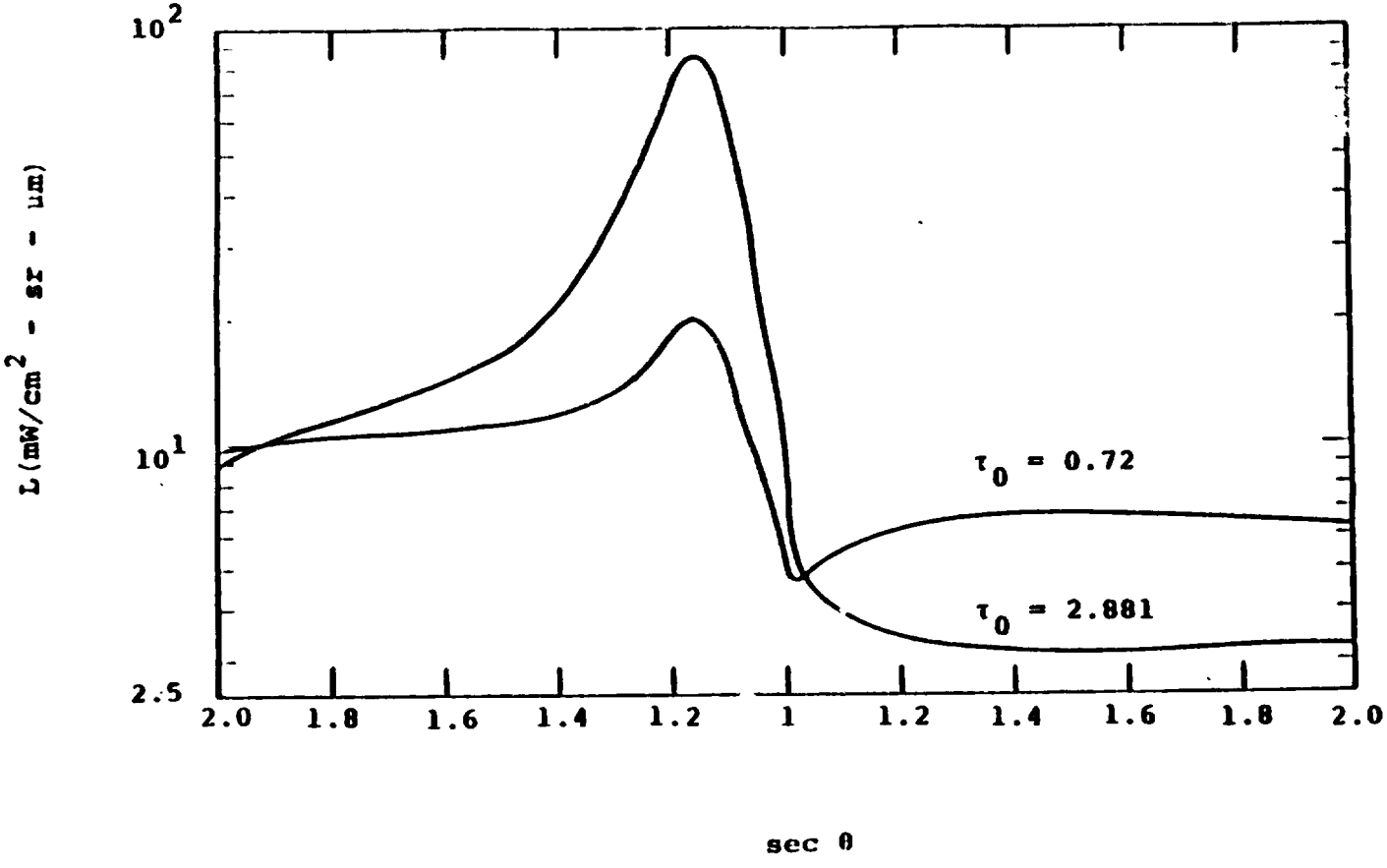

FIGURE 23. RADIANCE AT 0.380 μm vs. THE SECANT OF THE NADIR VIEW ANGLE IN THE SOLAR PLANE FOR A "COSINE-SINE-SQUARED" TARGET AND A VEGETATIVE BACKGROUND. SOLAR ZENITH ANGLE = 30°

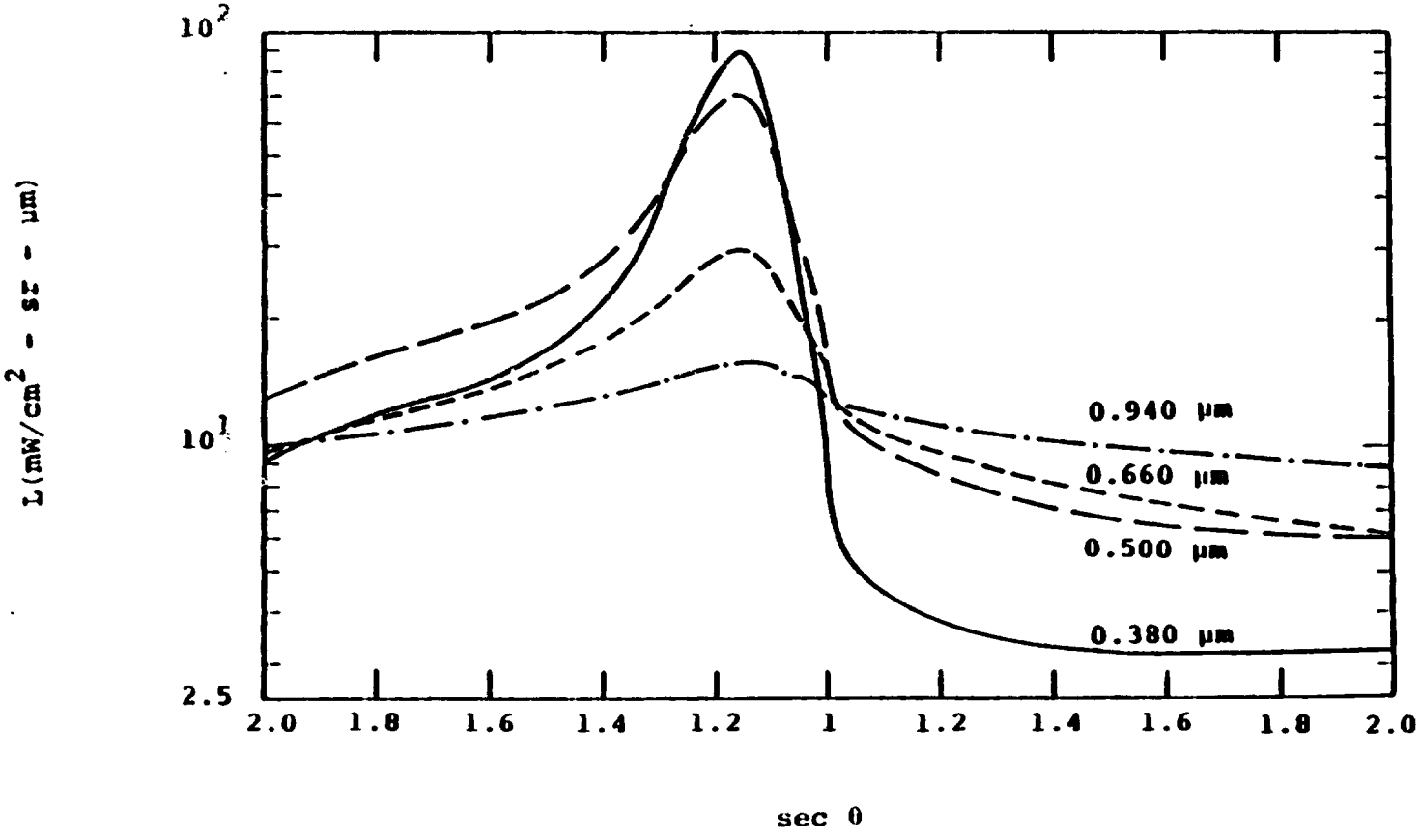

FIGURE 24. RADIANCE vs. THE SECANT OF THE NADIR VIEW ANGLE IN THE SOLAR PLANE AT FOUR WAVELENGTHS FOR A WHITE DIFFUSE TARGET AND A VEGETATIVE BACKGROUND. SOLAR ZENITH ANGLE = 30°. VISUAL RANGE = 2 km.

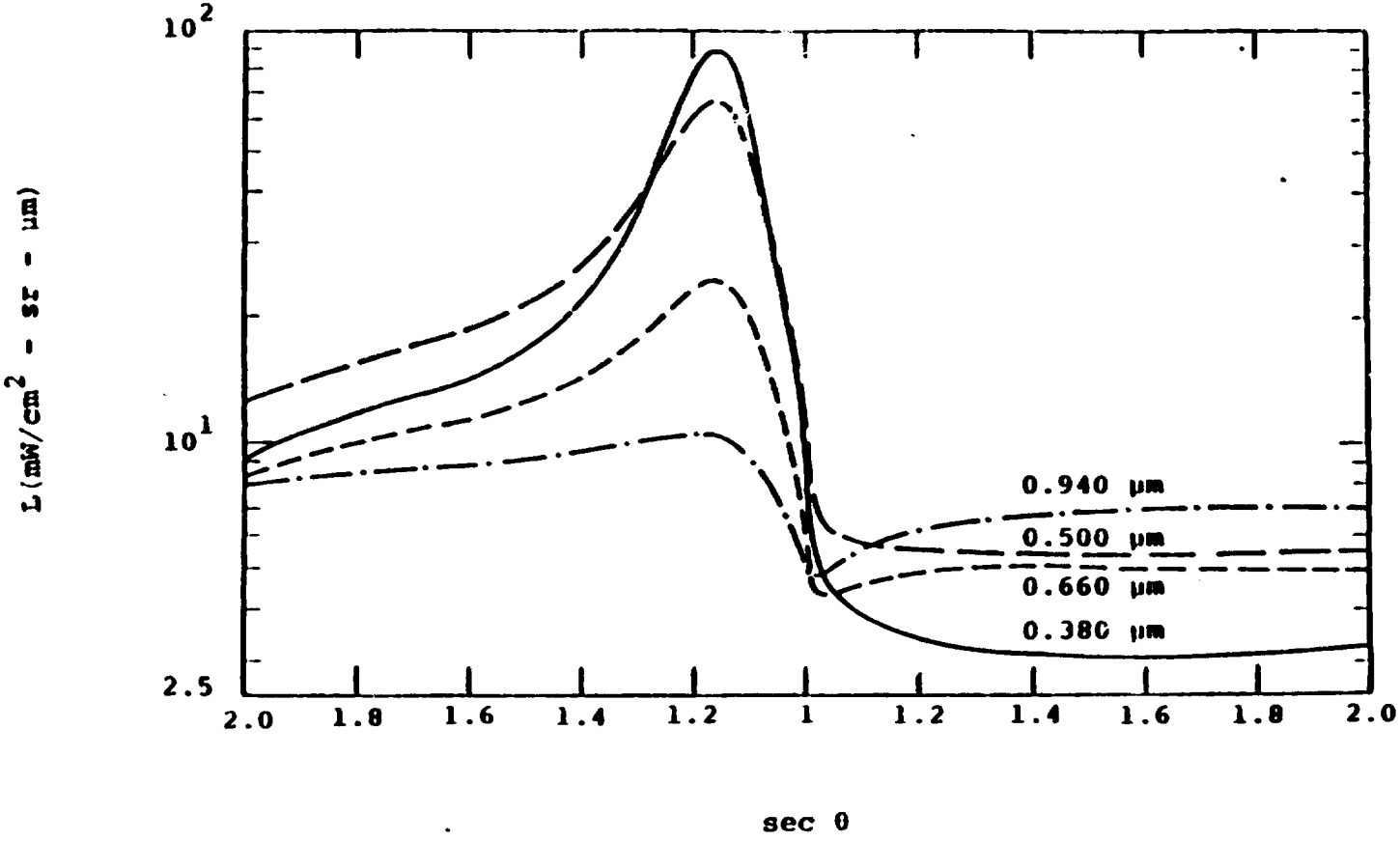

FIGURE 25. RADIANCE vs. THE SECANT OF THE NADIR VIEW ANGLE IN THE SOLAR PLANE AT FOUR WAVELENGTHS FOR A "COSINE-SINE-SQUARED" TARGET AND A VEGETATIVE BACKGROUND. SOLAR ZENITH ANGLE = 30°. VISUAL RANGE = 2 km.

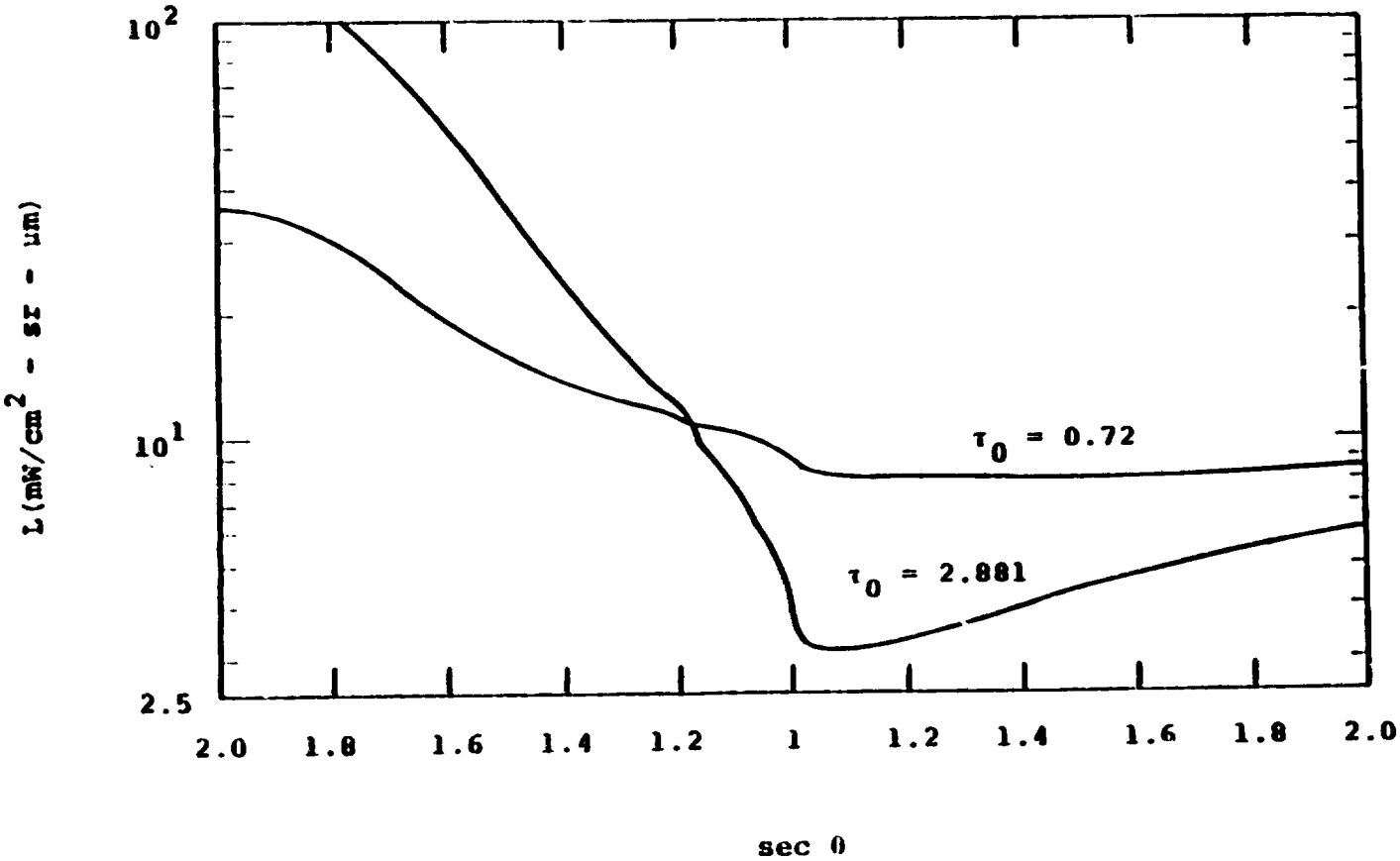

FIGURE 26. RADIANCE AT 0.380 μm vs. THE SECANT OF THE NADIR VIEW ANGLE IN THE SOLAR PLANE FOR A WHITE DIFFUSE TARGET AND A VEGETATIVE BACKGROUND. SOLAR ZENITH ANGLE = 60°.

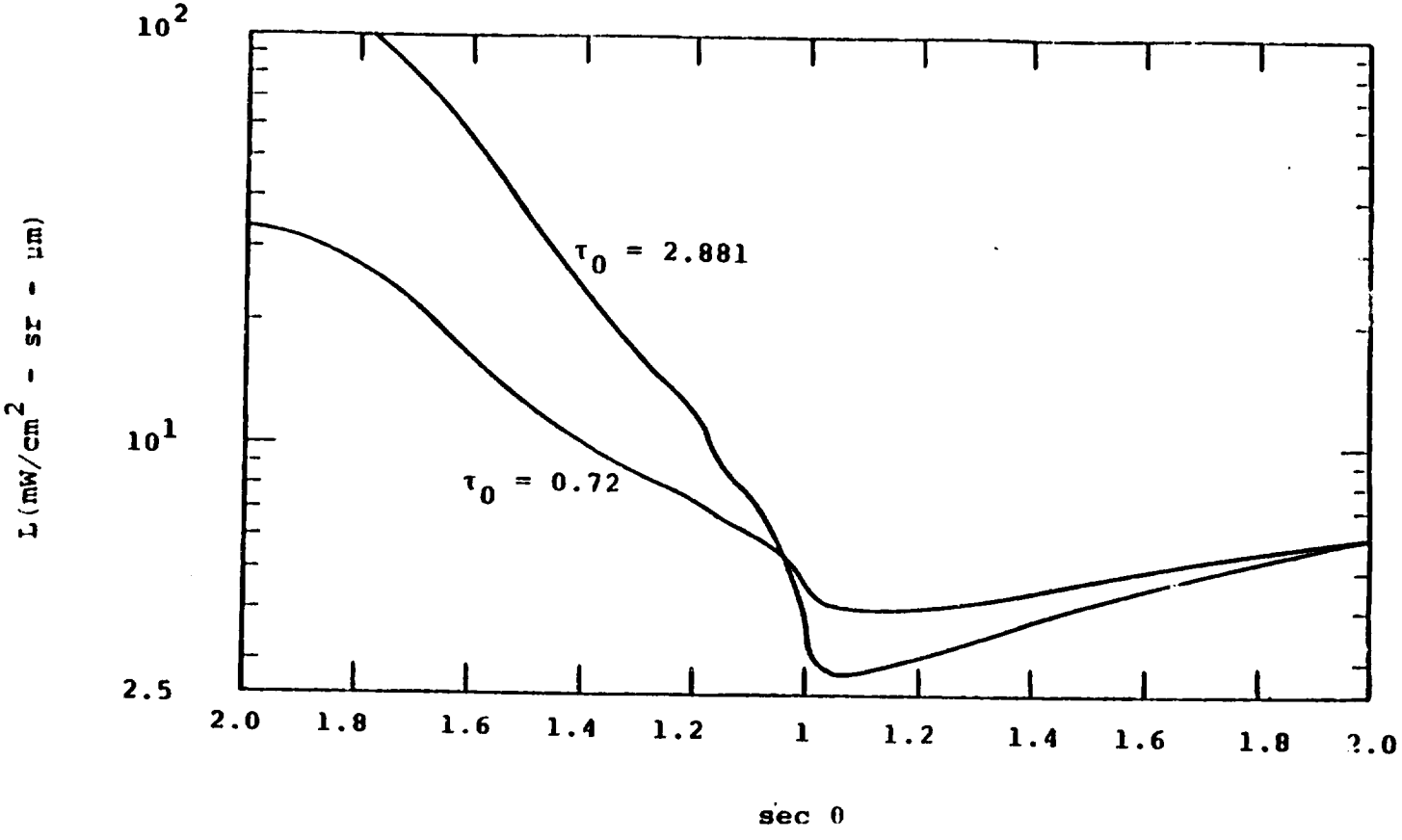

FIGURE 27. RADIANCE AT 0.380 μm vs. THE SECANT OF THE NADIR VIEW ANGLE IN THE SOLAR PLANE FOR A "COSINE" TARGET AND A VEGETATIVE BACKGROUND. SOLAR ZENITH ANGLE = 60°.

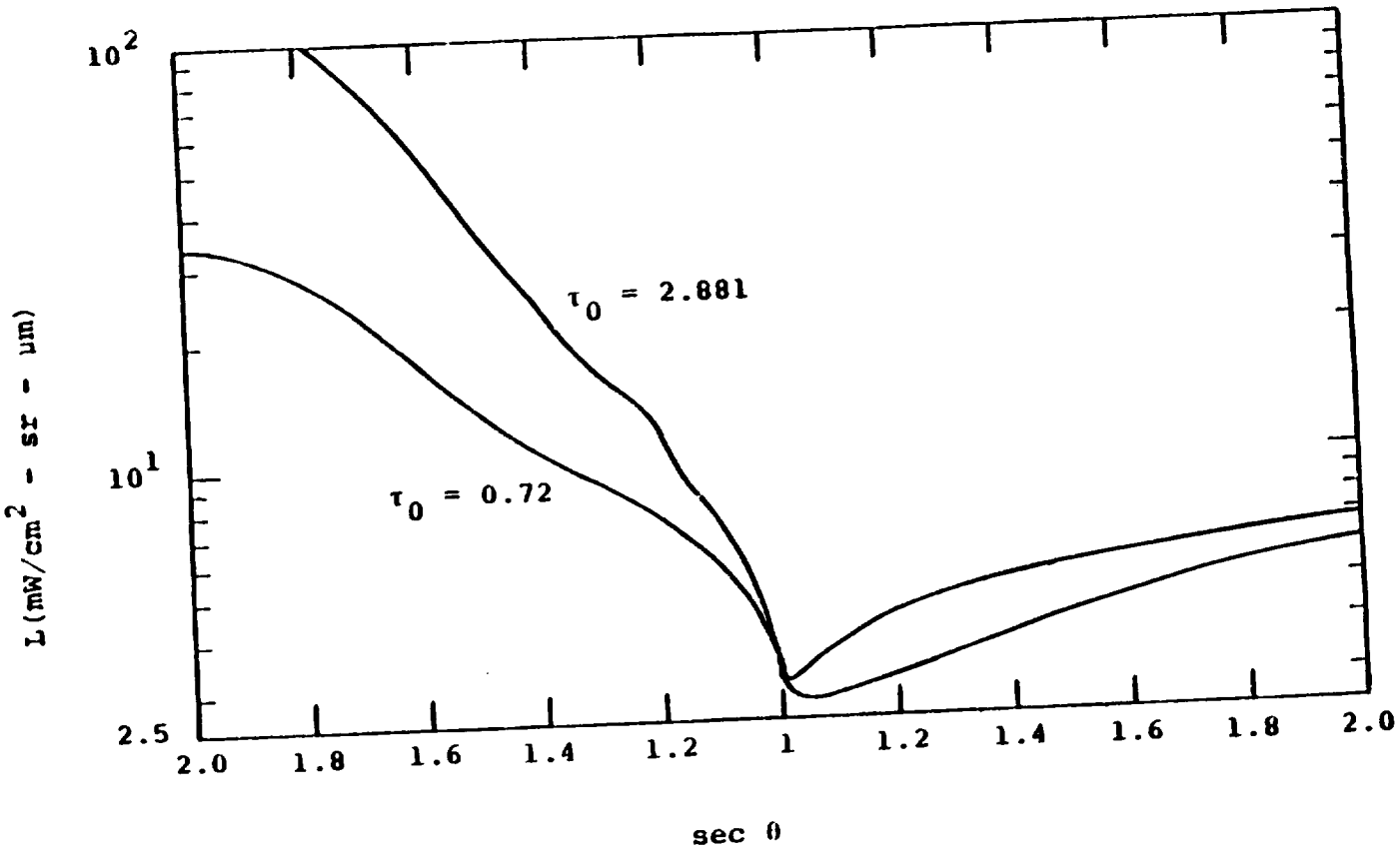

FIGURE 28. RADIANCE AT 0.380 μm vs. THE SECANT OF THE NADIR VIEW ANGLE IN THE SOLAR PLANE FOR A "cos θ sin^{2}θ" TARGET AND A VEGETATIVE BACKGROUND. SOLAR ZENITH ANGLE = 60°.

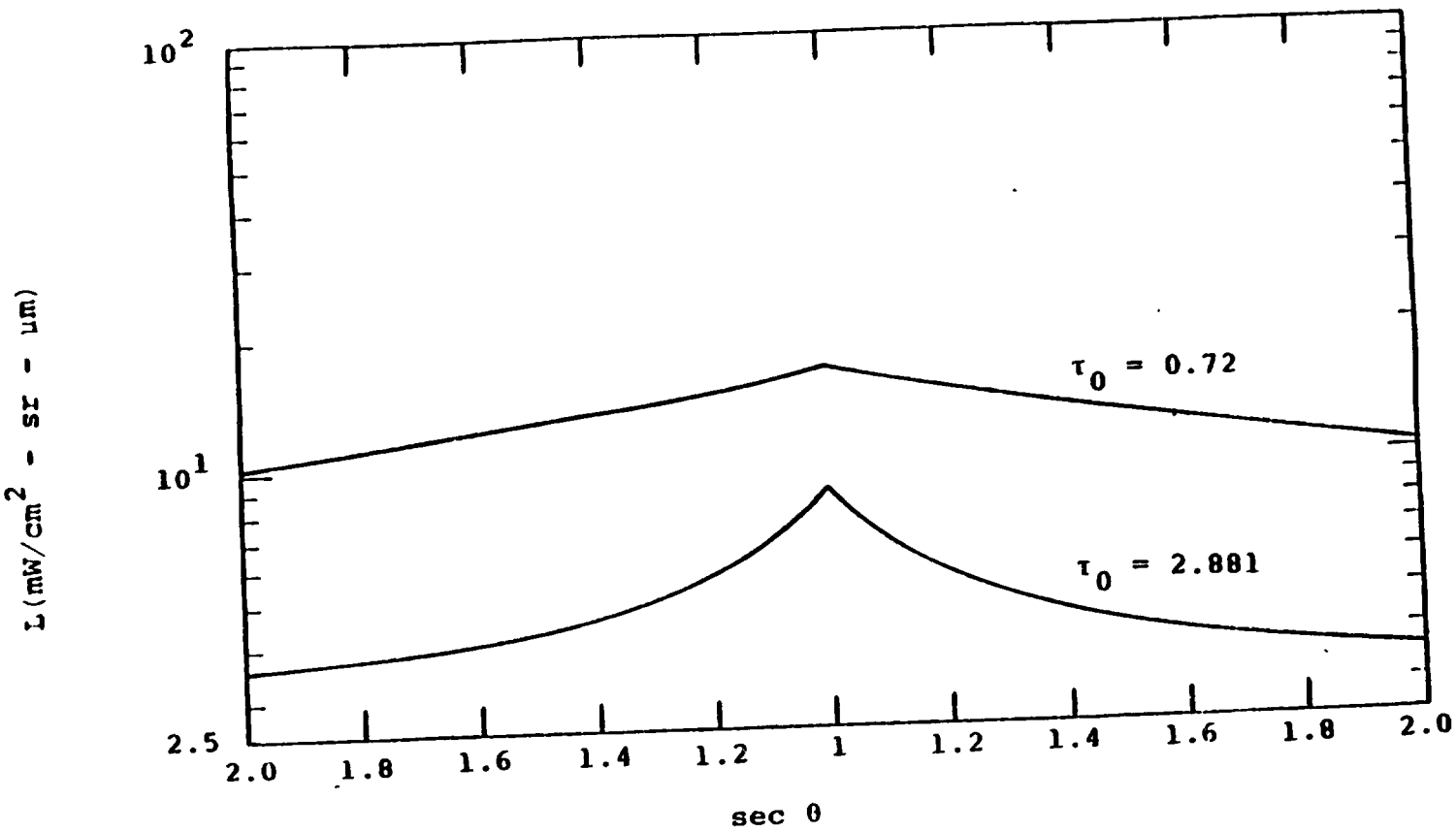

FIGURE 29. RADIANCE AT 0.380 μm VS. THE SECANT OF THE NADIR VIEW ANGLE PERPENDICULAR TO THE SOLAR PLANE FOR A WHITE DIFFUSE TARGET AND A VEGETATIVE BACKGROUND. SOLAR ZENITH ANGLE = 30°.

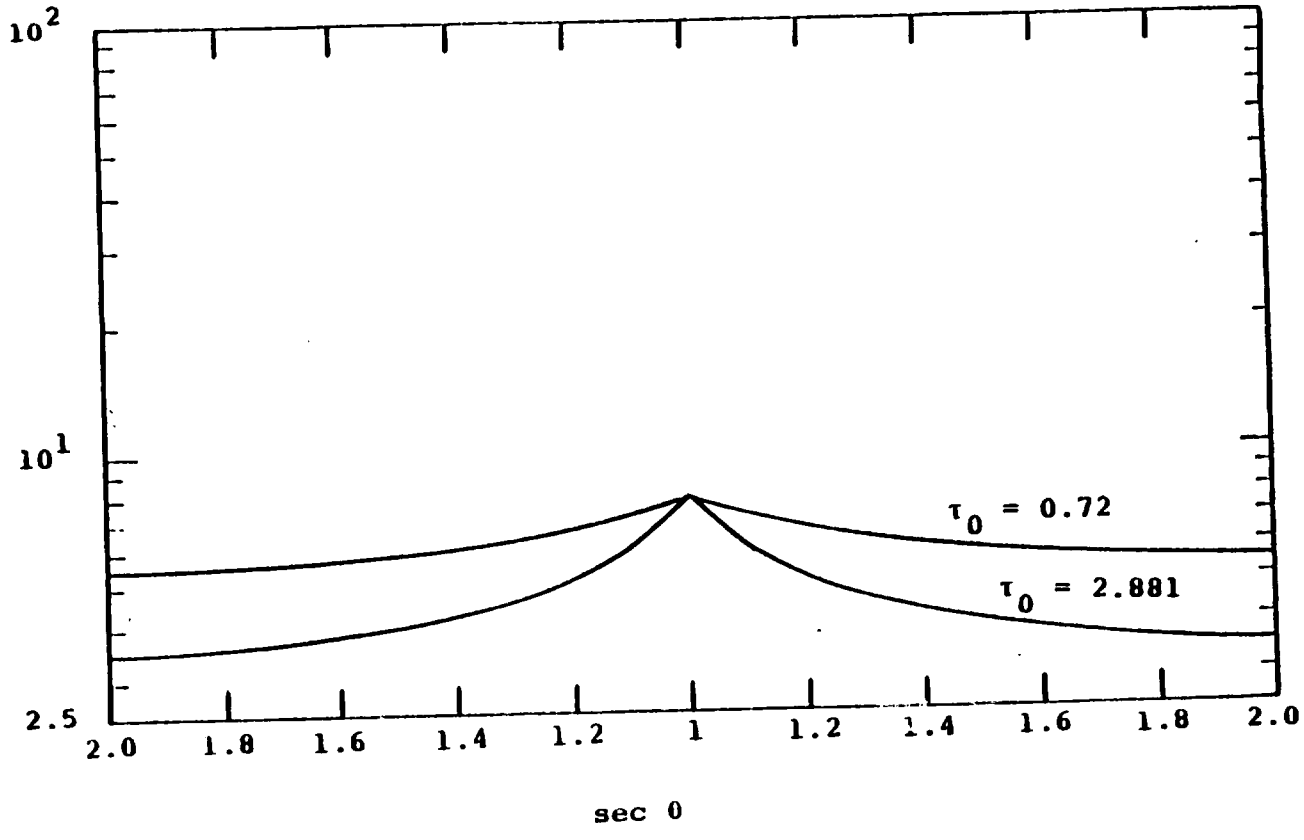

FIGURE 30. RADIANCE AT 0.380 μm vs. THE SECANT OF THE NADIR VIEW ANGLE PERPENDICULAR TO THE SOLAR PLANE FOR A "COSINE" TARGET AND A VEGETATIVE BACKGROUND. SOLAR ZENITH ANGLE = 30°.

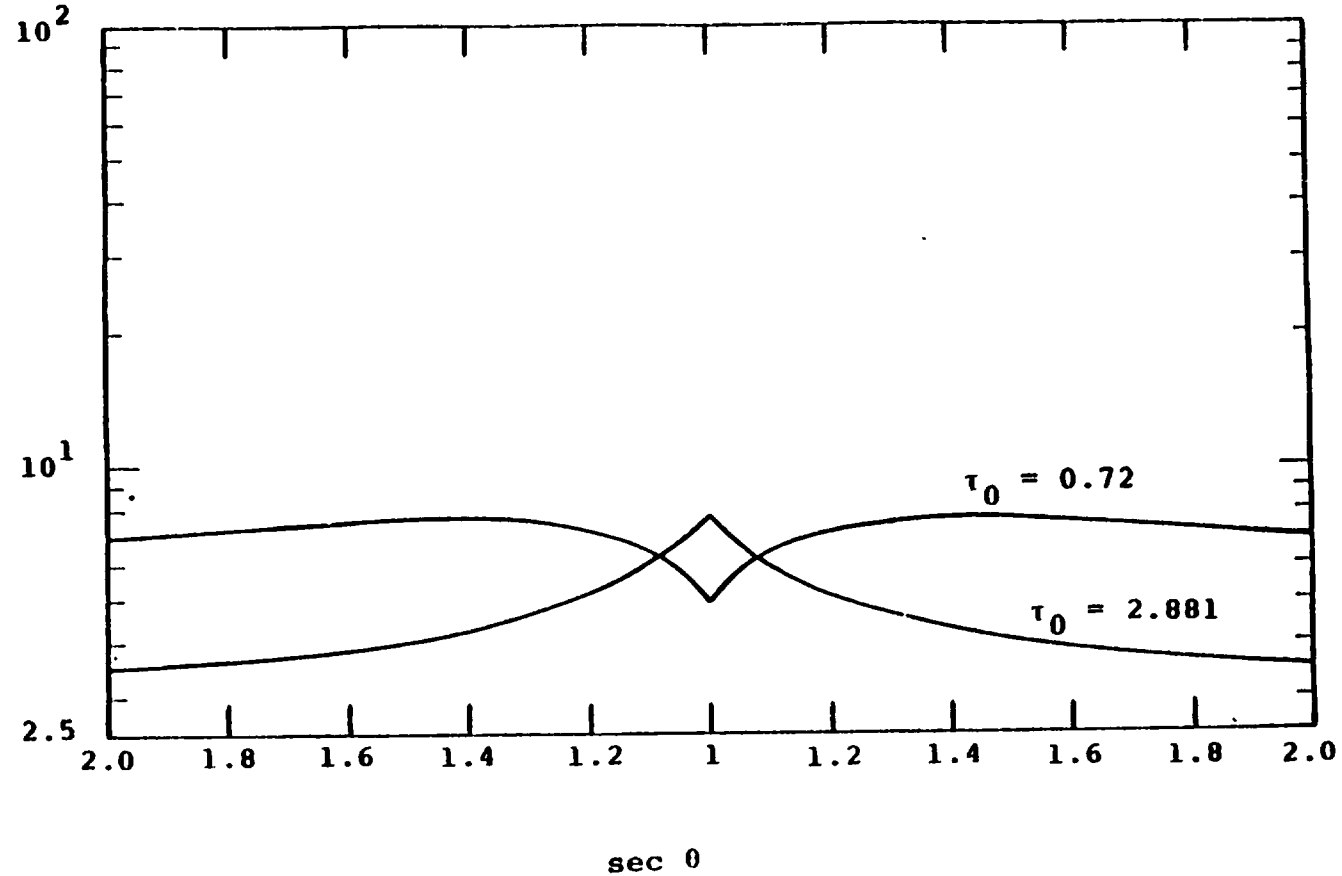

FIGURE 31. RADIANCE AT 0.380 μm vs. THE SECANT OF THE NADIR VIEW ANGLE PERPENDICULAR TO THE SOLAR PLANE FOR A "COSINE-SINE-SQUARED" TARGET AND A VEGETATIVE BACKGROUND. SOLAR ZENITH ANGLE = 30°.

4
ATMOSPHERIC CORRECTION ALGORITHMS

In this section we will consider several algorithms which can be used to determine the spectral optical thickness of the atmosphere. It is the atmospheric optical thickness which is of major importance in the calculation of the radiation field. This factor was clearly illustrated in the MRS simulation plots in the previous section.

4.1 HOMOGENEOUS ATMOSPHERE - DIFFUSE TARGETS

The most elementary case is that in which the atmosphere is uniform in the horizontal plane and for targets which are Lambertian. Because we are mainly concerned with the variation in the nadir view angle for the MRS, we will suppress many of the other parameters in the notation. The radiances at the sensor for two neighboring small targets are the following:

$$L_1(\tau_0,\theta) = L_{01}(\tau_0)T_1(\tau_0,\theta) + L_{P_1}(\tau_0,\theta) \tag{12}$$

and

$$L_2(\tau_0,\theta) = L_{02}(\tau_0)T_2(\tau_0,\theta) + L_{P_2}(\tau_0,\theta) \tag{13}$$

If the atmosphere is uniform and the angular field of view is small enough so that there is a negligible effect of one target on another via atmospheric scattering then the transmittances and path radiances are equal. If we now form a difference function from Eq. 12 and 13 we get

$$D(\tau_0,\theta) = D_0(\tau_0)T(\tau_0,\theta). \qquad (14)$$

The transmittance in Eq. 14 is given by

$$T(\tau_0,\theta) = e^{-\tau_0 \sec \theta} \qquad (15)$$

so that we get the following equation for the logarithm of the difference function for two diffuse targets:

$$\ln D(\tau_0,\theta) = \ln D_0(\tau_0) - \tau_0 \sec \theta \qquad (16)$$

The left-hand side of Eq. 16 is a measurable quantity for each spectral band of the MRS and, the nadir angle θ is always known for each corresponding radiance. Thus, if one plots the logarithm of the difference function vs. the secant of the nadir view angle, a straight line results, the slope of which provides a value of the spectral optical thickness τ_0. It is not important what the surface difference function $D_0(\tau_0)$ is because that only determines the intercept. For this reason we will plot the logarithm of the spectral transmittance of a very hazy (V = 2 km) atmosphere vs. the secant of the nadir view angle in Figure 32. The slope is greater for the shorter wavelength curve because of the longer optical thickness at that wavelength.

If we now consider one wavelength, say the one at 0.380 μm, we can plot the logarithm of the transmittances vs. the secant of the nadir view angle for three atmospheres. This is illustrated in Figure 33 for uniform atmospheres with horizontal visual ranges of 2 km, 13 km, and 40 km.

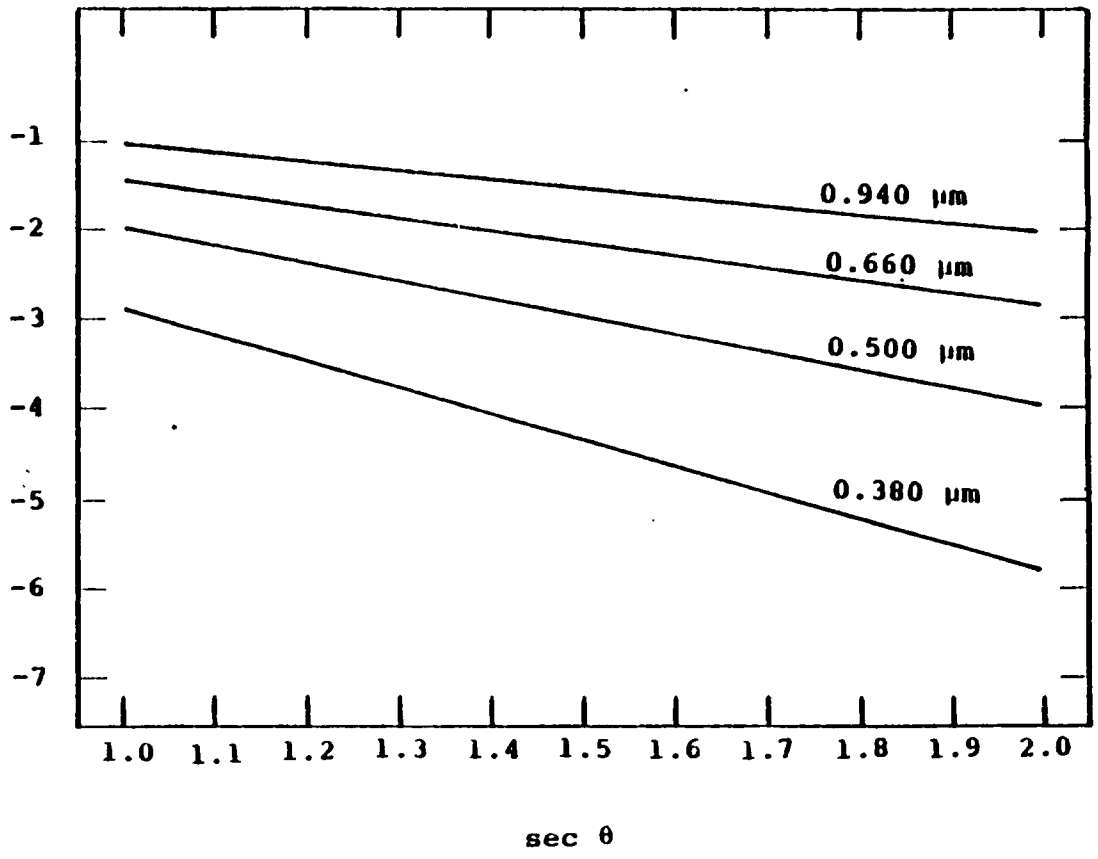

FIGURE 32. LOGARITHM OF THE TRANSMITTANCE vs. THE SECANT OF THE NADIR VIEW ANGLE FOR FOUR MRS WAVELENGTHS AND FOR A VERY HAZY (V = 2 km) UNIFORM ATMOSPHERE.

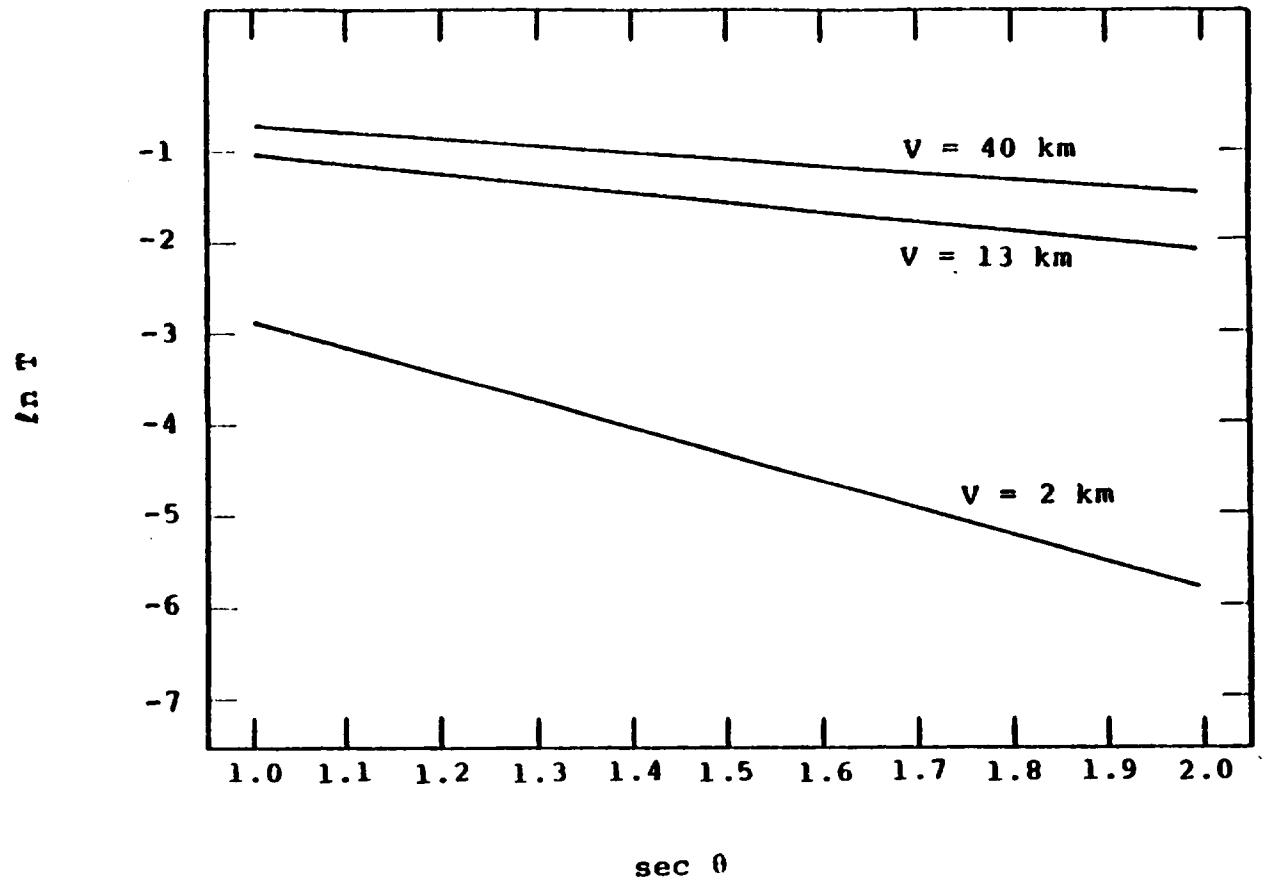

FIGURE 33. LOGARITHM OF THE TRANSMITTANCE vs. THE SECANT OF THE NADIR VIEW ANGLE FOR THREE ATMOSPHERES AT A WAVELENGTH OF 0.380 μm.

4.2 INHOMOGENEOUS ATMOSPHERE - DIFFUSE TARGETS

The question arises, how does the atmospheric transmittance vary with the secant of the nadir view angle if the atmosphere is not uniform? Figure 34 illustrates the situation in which a satellite passes over a target and receives radiation from various angles and therefore from various parts of a spatially variable atmosphere. In this case we have illustrated a situation in which there is an increase in the aerosol content in a horizontal plane but in which it is homogeneous in any vertical plane up to some constant height H. It is assumed that the molecular component is horizontally homogeneous everywhere. It should be noted that atmospheric refraction is negligible for the angle to be considered.

We can now consider a simple model of a haze layer. Figure 35 depicts the geometry of the optical properties of the haze. The arbitrary origin is at x = 0 and the target to be considered is located at x. We will consider the visual range V(x) to be represented as the following:

$$V(x) = V(0) + \frac{1}{1!}\frac{dV}{dx}x + \frac{1}{2!}\frac{d^2V}{dx^2}x^2 + \ldots \qquad (17)$$

Here we shall limit our discussion to a "linear" haze, i.e. one which is given by

$$V(x) = V(0) + \frac{V(\ell) - V(0)}{\ell}x \qquad (18)$$

where V(0) is the visual range at the origin and ℓ is the

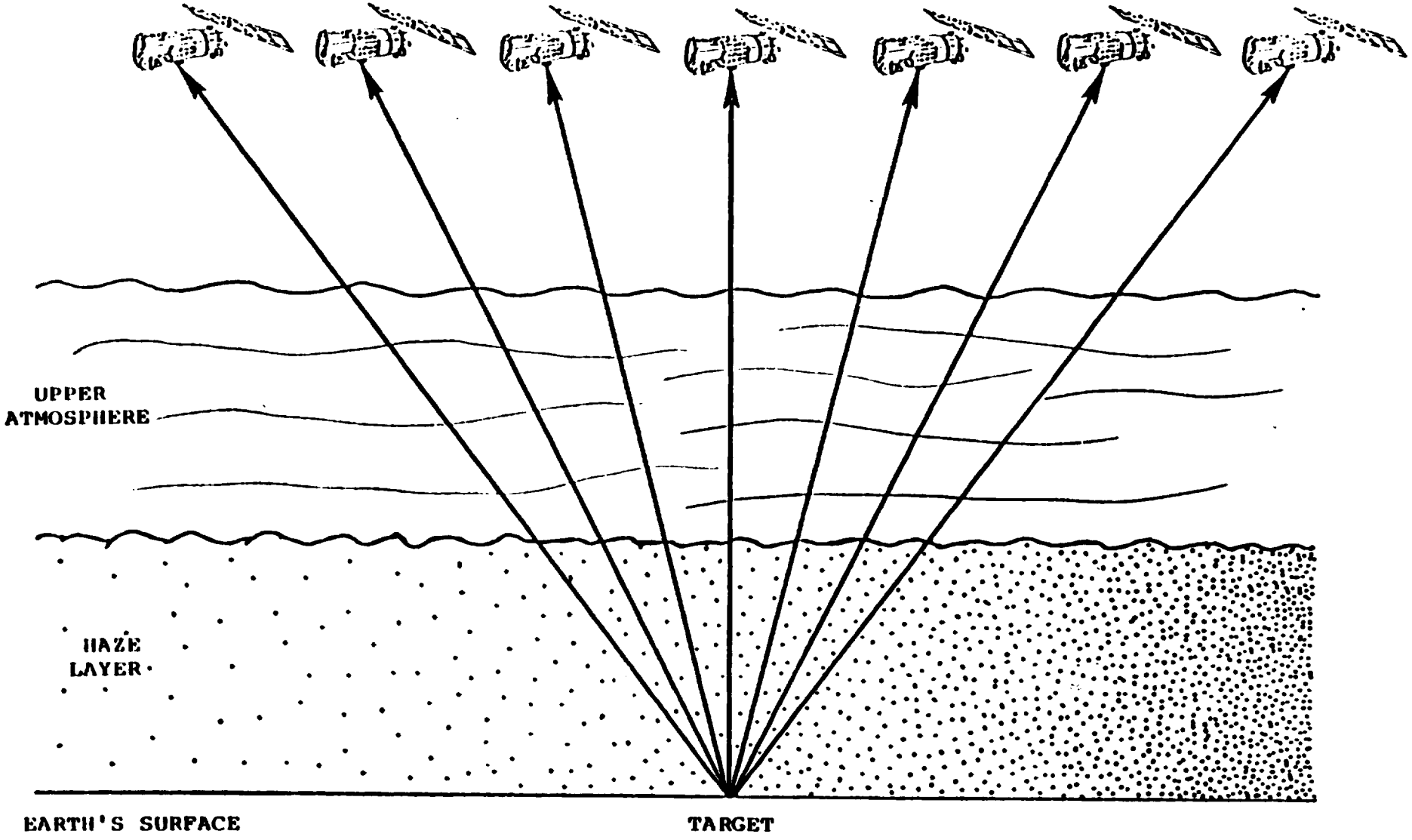

FIGURE 34. SATELLITE OBSERVATION OF TARGET THROUGH AN INHOMOGENEOUS ATMOSPHERIC HAZE.

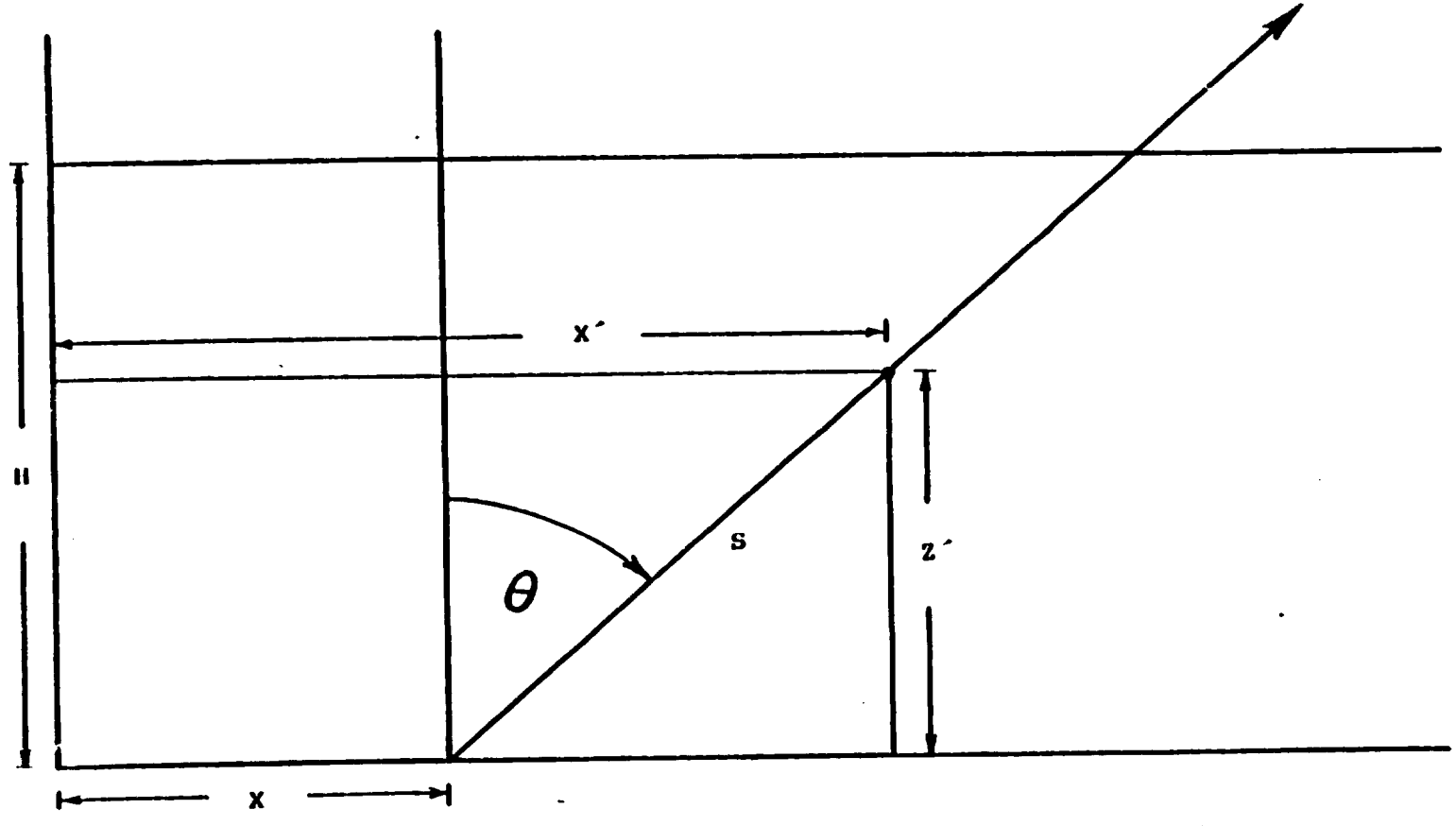

FIGURE 35. GEOMETRY FOR THE ANALYSIS OF INHOMOGENEOUS ATMOSPHERES.

scale length such that $V(\ell)$ is the visual range at ℓ.

The optical thickness along the path s for the point x at the surface is given by

$$\tau_0(x,\theta) = \int_0^\infty \kappa(x',z')ds$$

$$= \sec\theta \int_0^\infty \kappa(x',z')dz'. \qquad (19)$$

The total volume extinction coefficient $\kappa(x',z')$ is then

$$\kappa(x',z') = \kappa_A(x',z') + \kappa_G(z')$$

$$= \frac{\ell n\ 50}{V(x')} * \qquad (20)$$

where Eq. 20 is the usual relationship connecting extinction coefficient with visual range and it is to be understood that Eq. 20 holds for the wavelength $\lambda = 0.55$ um. The $\kappa_A(x',z')$ term is the aerosol volume extinction coefficient and $\kappa_G(z')$ is the Rayleigh volume extinction coefficient. Using relation 18 in Eq. 19 we get

*Note: $\ell n\ 50 = 3.912$. This arises from the use of a 2% contrast for the human eye.

$$\tau_0(x,\theta) = \ell n\ 50 \sec\theta \int_0^H \frac{dz'}{V(0) + \frac{V(x) - V(0)}{x} x'}$$

$$+ (\tau_G - \kappa_G(0)H)\sec\theta \qquad (21)$$

where

$$\tau_G = \int_0^\infty \kappa_G(z')dz' \qquad (22)$$

and $\kappa_G(0)$ is the value of $\kappa_G(z)$ at $z = 0$. According to Figure 35

$$x' = x + z' \tan\theta \qquad (23)$$

and using this relation in Eq. 21 gives us the following:

$$\tau_0(x,\theta) = \frac{x \sec\theta\ \ell n\ 50}{\left[V(x) - V(0)\right]\tan\theta} \ell n \left[1 + \frac{H\left(V(x) - V(0)\right)\tan\theta}{x\ V(x)}\right]$$

$$+ \left(\tau_G - \kappa_G(0)H\right)\sec\theta \qquad (24)$$

Equation 20 describes the total optical thickness at an angle θ for a "linear" haze. It is interesting to see what this becomes as $\theta \to 0$. Define

$$\Delta = \frac{H\,[V(x) - V(0)]\,\tan\theta}{x\,V(x)}\,, \tag{25}$$

then, as $\Delta \to 0$ Eq. 24 becomes

$$\tau_0(x,\theta) = \frac{H \sec\theta\ \ell n\ 50}{V(x)\ \Delta}\left(\Delta - \frac{\Delta^2}{2} + \ldots\right)$$

$$+\left(\tau_G - \kappa_G(0)\ H\right)\sec\theta, \tag{26}$$

or

$$\tau_0(x,0) = \frac{H\ \ell n\ 50}{V(x)} + \tau_G - \kappa_G(0)\ H. \tag{27}$$

For other wavelengths we must consider a model for the haze. The model devised by Elterman [12] will be used here for the spectral dependence. Thus, we have for the general, wavelength - dependent optical thickness of an inhomogeneous haze

$$\tau_0(\lambda,x,\theta) = \frac{x \sec\theta \ \ell n\ 50}{[V(x) - V(0)] \tan\theta} \frac{I(\lambda)}{I(\lambda_0)} \ell n \left[1 + \frac{H[V(x) - V(0)] \tan\theta}{x\ V(x)} \right]$$

$$+ \left[\tau_G(\lambda) - \kappa_G(0,\lambda_0) \frac{I(\lambda)}{I(\lambda_0)} H \right] \sec\theta \qquad (28)$$

where $\lambda_0 = 0.55$ μm and $I(\lambda)/I(\lambda_0)$ is given in Table 4.

TABLE 4. SPECTRAL FUNCTION $I(\lambda)/I(\lambda_0)$

λ (μm)	0.380	0.500	0.660	0.940
Function	1.4536	1.0876	0.799	0.5876

The value of $\kappa_G(0,\lambda_0) = 0.012$ km^{-1}. We will set the height of the haze layer to be 0.8621 km, a value which is consistent with a horizontal visual range of 2 km. We then establish this height for hazes of <u>all</u> visual ranges but adjust the aerosol densities so as to provide the correct optical thickness.

We can now determine the logarithm of the spectral transmittance as a function of the secant of the nadir view angle for various hazes, i.e. for different aerosol horizontal gradients. First, we consider the case where

$$\left.\begin{aligned} V(0) &= 40 \text{ km} \\ V(x) &= 2 \text{ km} \end{aligned}\right\} \quad \text{Case 1}$$

and then

$$\left.\begin{aligned} V(0) &= 40 \text{ km} \\ V(x) &= 10 \text{ km} \end{aligned}\right\} \quad \text{Case 2.}$$

both with several values of x. The logarithm of the transmittance is given by

$$\ell n\, T_0(\lambda,x,\theta) = -\tau_0(\lambda,x,\theta). \qquad (29)$$

It is assumed that the target is at the position x for which the visual range is V(x). In Figure 36 we consider a situation of varying x for one of the MRS bands. The solid line represents a change in visual range of 38 km in a distance of 30 km, or a gradient of 1.267 km/km. The large dash curve is for an x of 50 km and the small dash curve is for x = 100 km. The transmittance decreases quite rapidly as the view angle increases beyond 0°, especially for the large gradient situation. As $x \to \infty$ the curves should become straight lines as in the homogeneous cases. It is interesting to note that the maximum transmittance does not occur at $\theta = 0°$ but rather on the high visual range side of the plot. The slope changes rapidly near $\theta = 0°$ in a somewhat surprising manner. This can be easily seen if we plot the same set of curves on a highly magnified basis as in

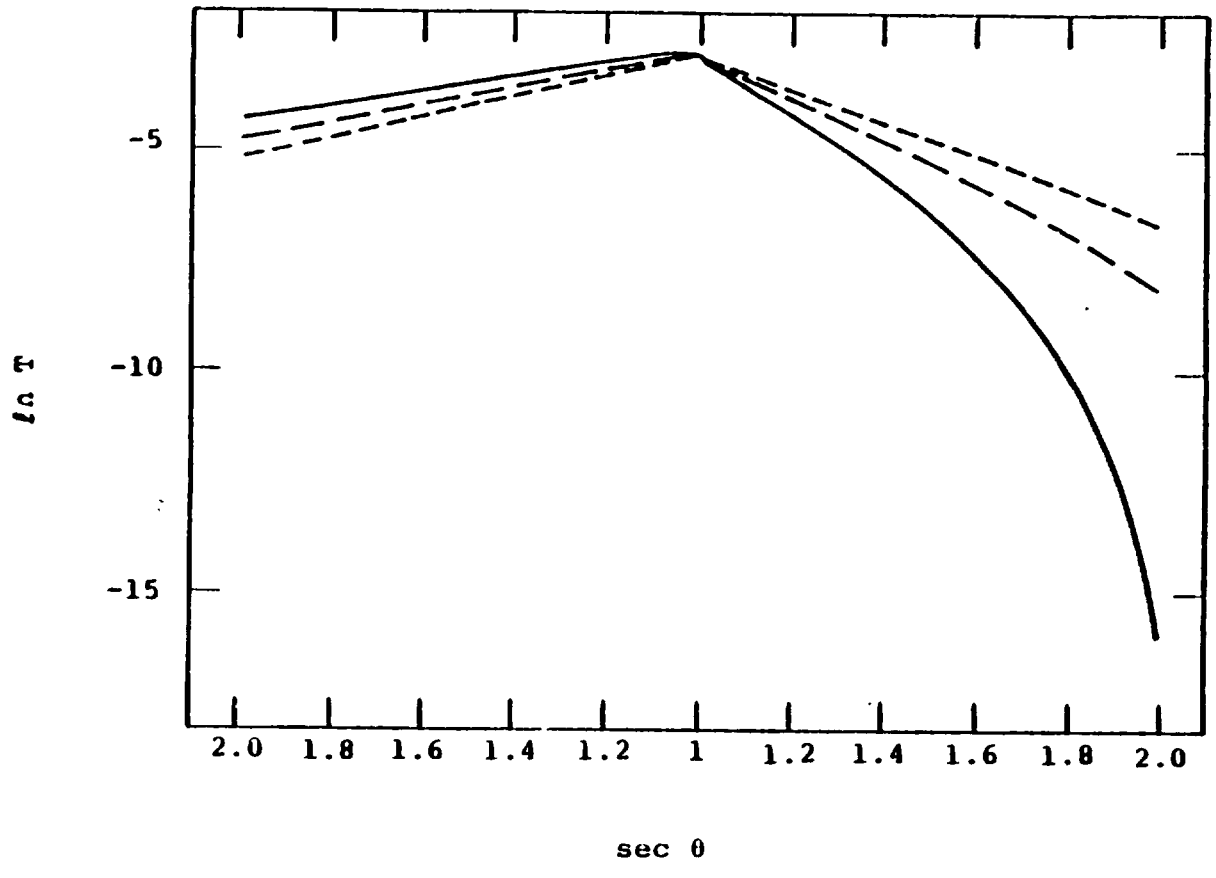

FIGURE 36. LOGARITHM OF THE TRANSMITTANCE vs. THE SECANT OF THE NADIR VIEW ANGLE FOR NON-UNIFORM ATMOSPHERE AT A WAVELENGTH OF 0.380 μm. VISUAL RANGE GRADIENTS ARE:

———————— 1.267 km/km

— — — — 0.760 km/km

---------- 0.380 km/km

Figure 37. It is easy to demonstrate that the slope of the curves at the inflection point ($\theta = 0°$) is infinite if x is finite. The optical thickness is larger for the shorter wavelengths than for the longer wavelengths. This effect is not surprising and is illustrated in Figure 38 for x = 30 km. In Figure 39 we illustrate the effect of a increased visual range at the point of observation $\left(V(x) = 10 \text{ km}\right)$ but with higher gradients than in the lower visual range $\left(V(x) = 2 \text{ km}\right)$ case. Finally, we can understand the behavior of the transmittance in terms of the distance x for the positive angles θ. This is illustrated in Figure 40 for sec θ = 1.0, 1.6, 1.9, and 2.0. As the distance x decreases the gradient increases and the transmittance decreases because of the large optical thickness.

From this analysis one can see that the spectral optical thickness of Earth's atmosphere can be determined if the transmittance can be measured as a function of the view angle.

4.3 HOMOGENEOUS ATMOSPHERE - NON-DIFFUSE TARGETS

Here we consider the more general situation in which the target is non-Lambertian. The basic "correction" algorithm is that of Eq. 14, i.e.

$$D(\tau_0,\theta) = D_0(\tau_0,\theta)T(\tau_0,\theta) \qquad (30)$$

where the intrinsic difference function $D_0(\tau_0,\theta)$ is now dependent upon the view angle θ. If one makes the assumption that the sky radiance is constant over the hemisphere then Eq. 30 becomes

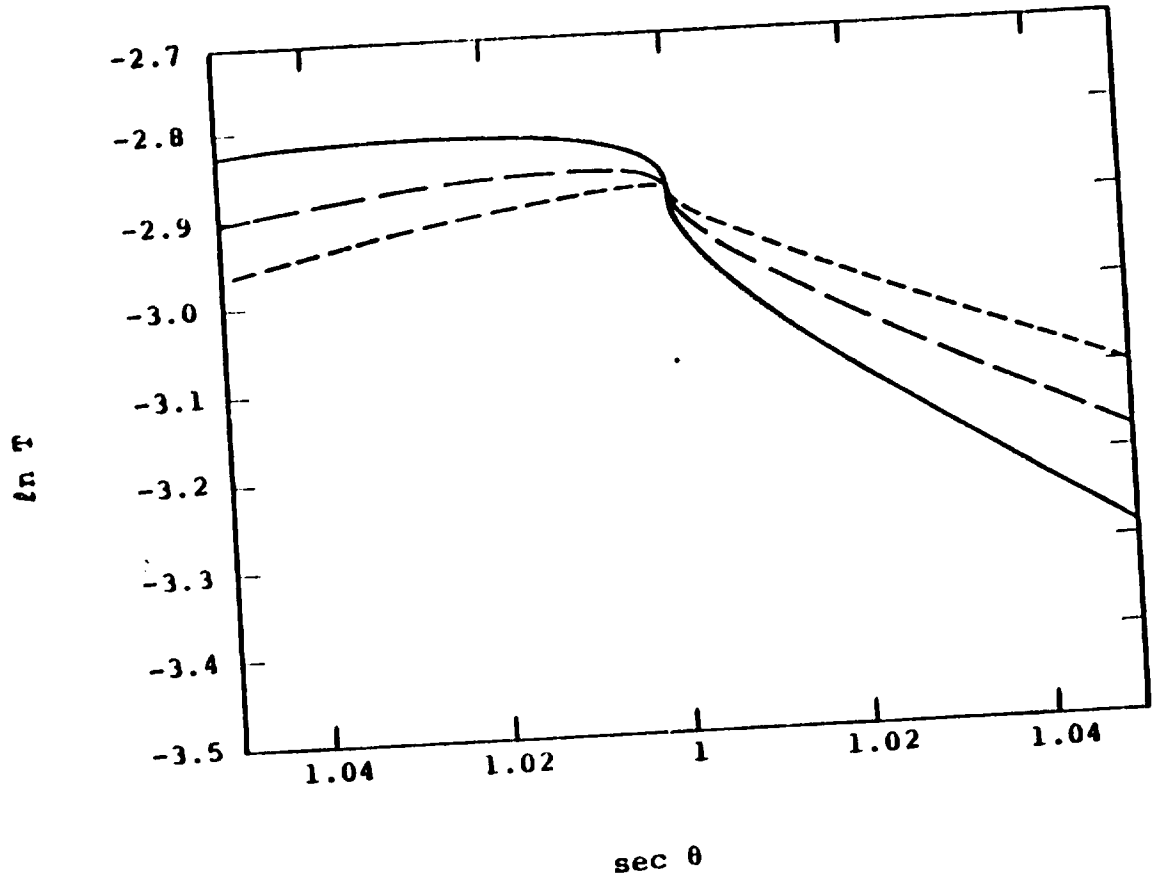

FIGURE 37. LORARITHM OF THE TRANSMITTANCE vs. THE SECANT OF THE NADIR VIEW ANGLE FOR A NON-UNIFORM ATMOSPHERE AT A WAVELENGTH OF 0.380 μm FOR THE RANGE $-17.75° \leq \theta \leq +17.75°$. VISUAL RANGE GRADIENTS ARE:

———————— 1.267 km/km

— — — — 0.760 km/km

---------- 0.380 km/km

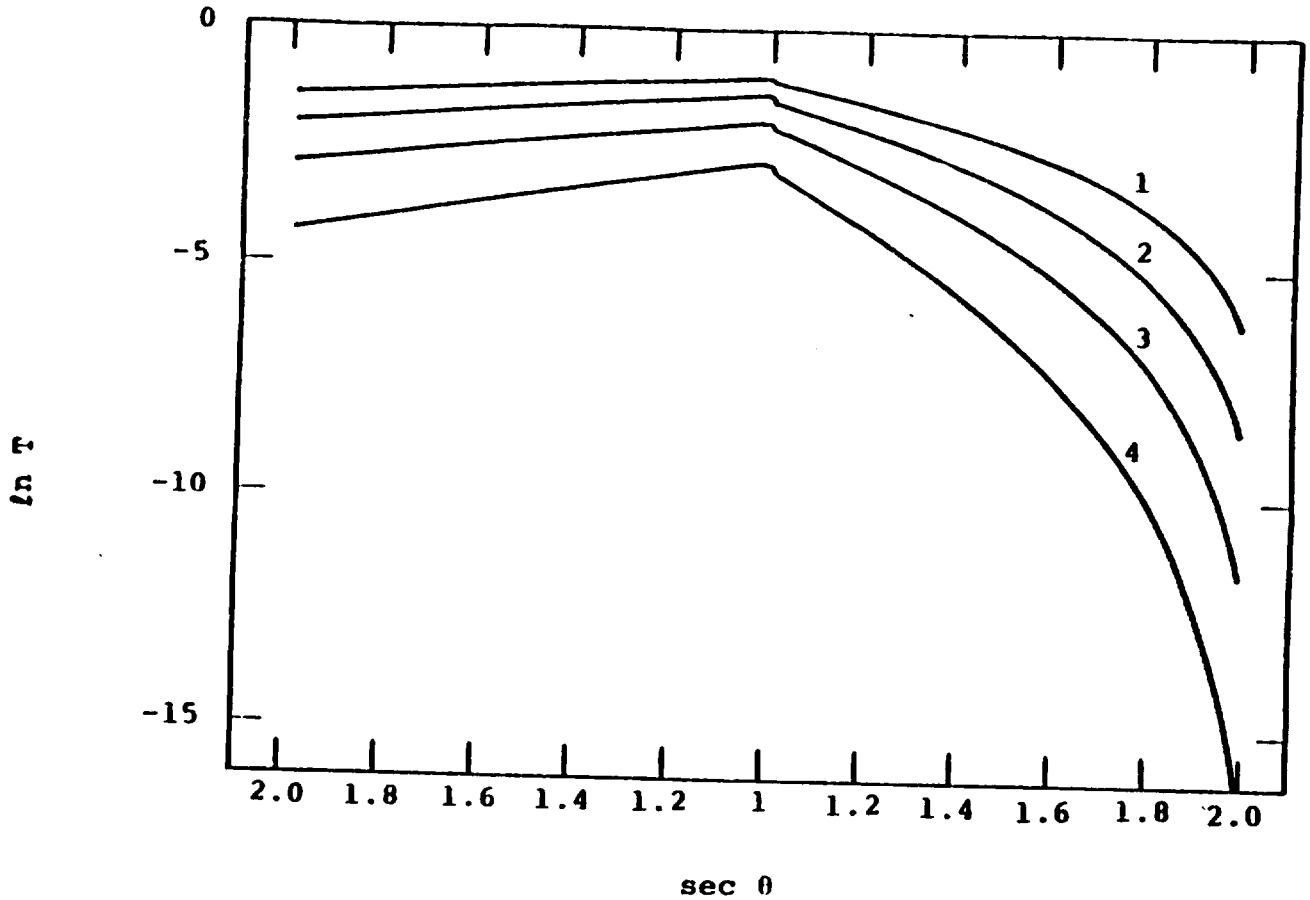

FIGURE 38. LOGARITHM OF THE TRANSMITTANCE vs. THE SECANT OF THE NADIR VIEW ANGLE FOR A NON-UNIFORM ATMOSPHERE FOR THE FOUR MRS WAVELENGTHS. VISUAL RANGE GRADIENT IS 1.267 km/km.

Curve 1 --- 0.940 μm

Curve 2 --- 0.660 μm

Curve 3 --- 0.500 μm

Curve 4 --- 0.380 μm

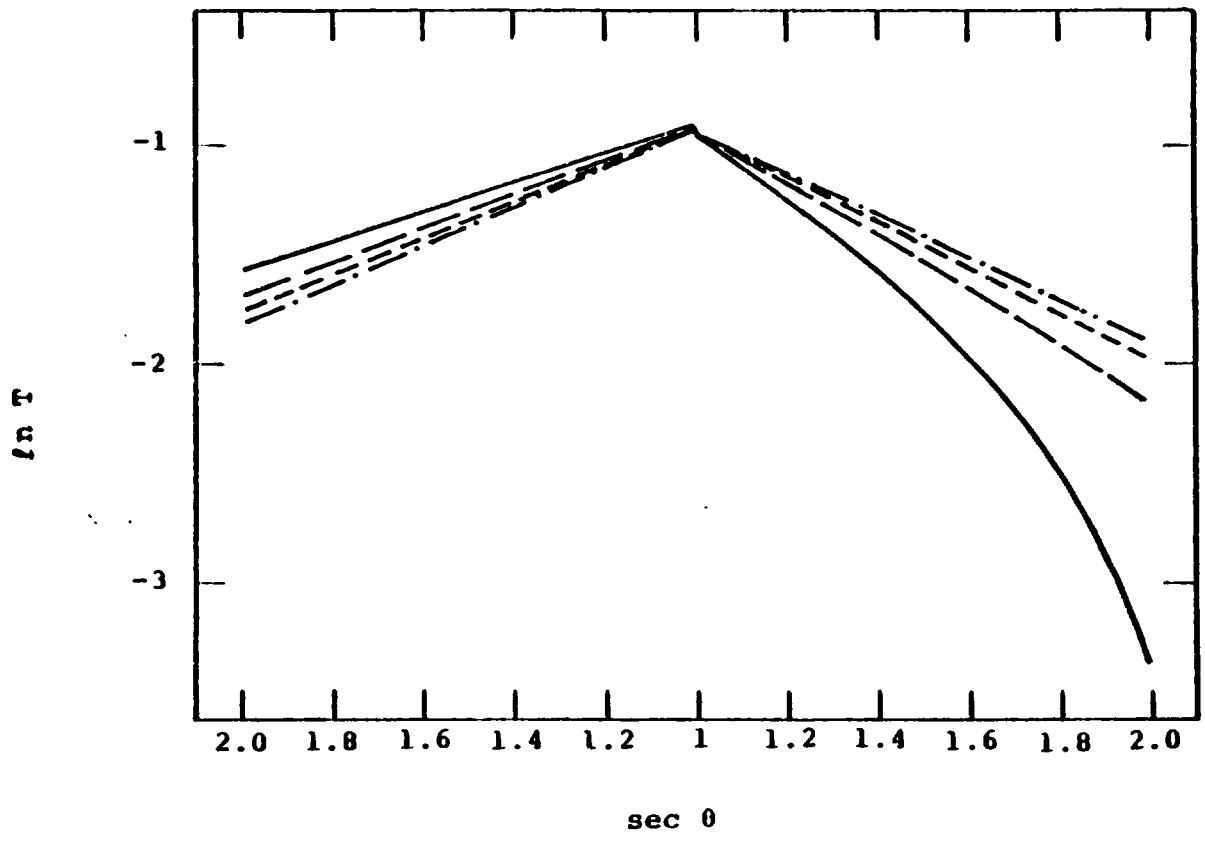

FIGURE 39. LOGARITHM OF THE TRANSMITTANCE vs. THE SECANT OF THE NADIR VIEW ANGLE FOR A NON-UNIFORM ATMOSPHERE FOR A WAVELENGTH OF 0.380 μm. VISUAL RANGE GRADIENTS ARE:

———————— 6.0 km/km
— — — — — — 3.0 km/km
— — — — — — 1.5 km/km
— — — — — — 0.6 km/km

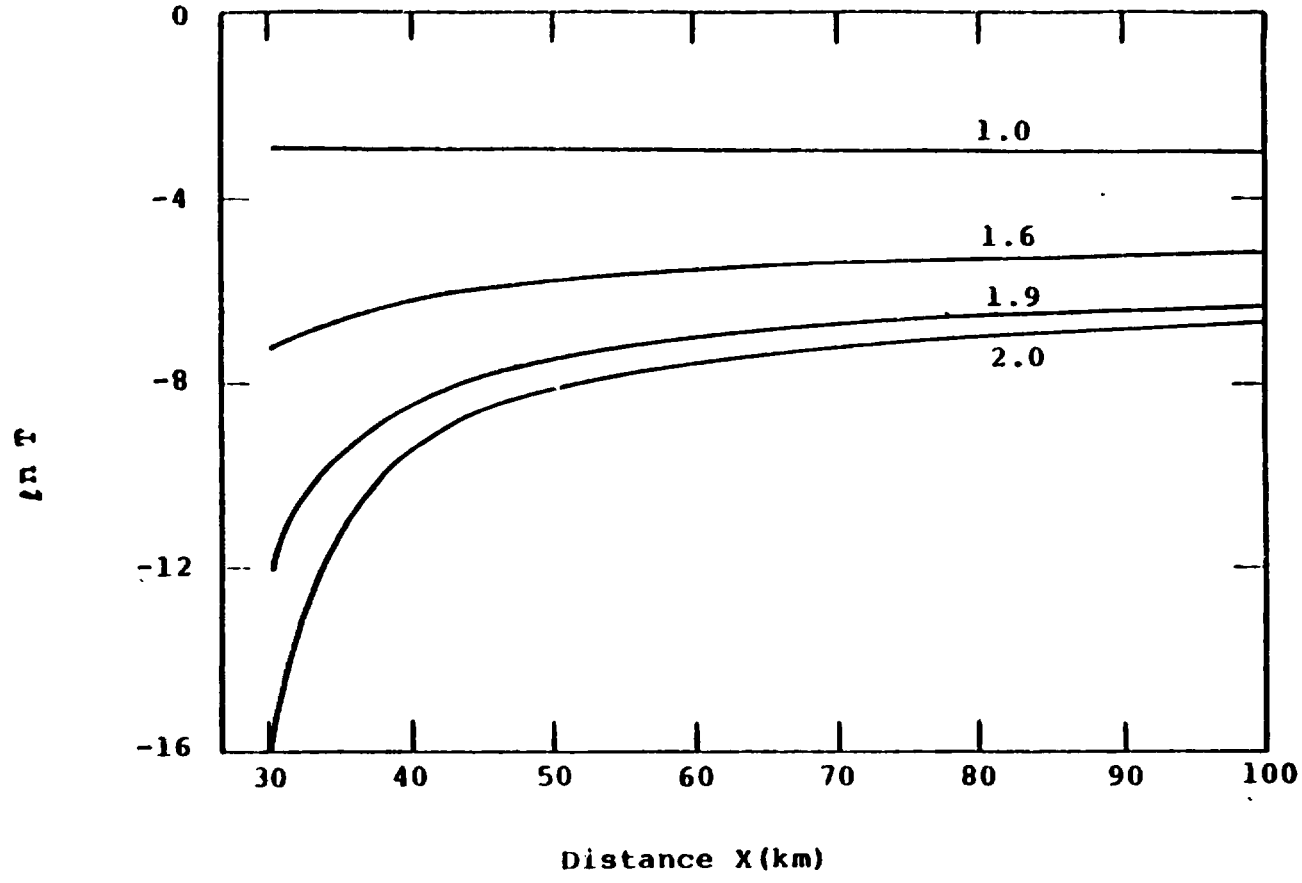

FIGURE 40. LOGARITHM OF THE TRANSMITTANCE vs. THE VISUAL RANGE SCALE DISTANCE X FOR FOUR SECANTS OF THE NADIR VIEW ANGLE. WAVELENGTH = 0.380 μm. V(0) = 40 km; V(X) = 2 km.

$$D(\tau_0,\theta) \cong \mu_0 E_0 e^{-\tau_0/\mu_0} T(\tau_0,\theta)\left[\rho_1(\mu,\phi, -\mu_0,\phi_0) - \rho_2(\mu,\phi, -\mu_0,\phi_0)\right]$$

$$+ L_s(\tau_0)T(\tau_0,\theta)\left[\rho_{1d}(\mu,\phi) - \rho_{2d}(\mu,\phi)\right] \qquad (31)$$

where $L_s(\tau_0)$ is the constant sky radiance and the $\rho_{id}(\mu,\phi)$ are the directional reflectances given by

$$\rho_{id}(\mu,\phi) = \int_0^{2\pi}\int_0^1 \mu' \rho_i(\mu,\phi,\mu',\phi')d\mu' d\phi'. \qquad (32)$$

In order to illustrate the variation in $D(\tau_0,\theta)$ with sec θ we will only consider the direct solar contribution, that is, the first part of Eq. 31. Figure 41 illustrates the variation in the difference function with the secant of the nadir view angle for two Lambertian targets and three visual ranges. The solar zenith angle is 60° but is of little importance except insofar as the absolute magnitude of the function is concerned. What Figure 41 indicates is just the variation of the transmittance along the line of sight as a function of the secant function. In Figure 42 we display the difference function for a diffuse surface and a surface with a cosine variation. From these two figures one can easily see a large difference in the set of curves for the diffuse pair of targets and the diffuse-cosine target combination. In Figure 43 we illustrate a variation in the difference function for a combination of a diffuse target and one with a $\cos\theta \sin^2\theta$ variation. The

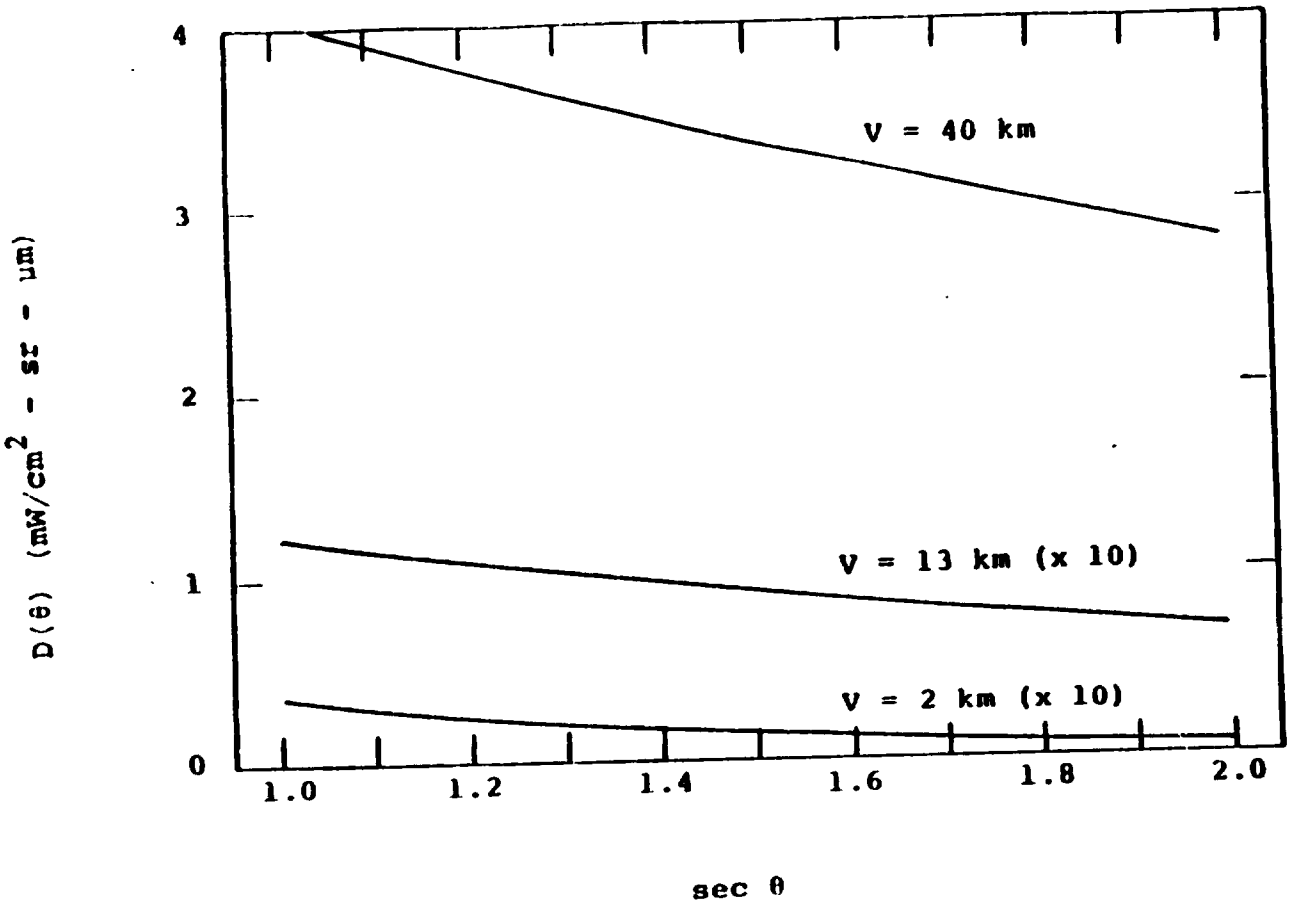

FIGURE 41. VARIATION OF THE DIFFERENCE FUNCTION WITH THE SECANT OF THE NADIR VIEW ANGLE FOR THREE UNIFORM ATMOSPHERES AT A WAVELENGTH OF 0.500 μm.

$\rho_1 = 0.8$

$\rho_2 = 0.4$

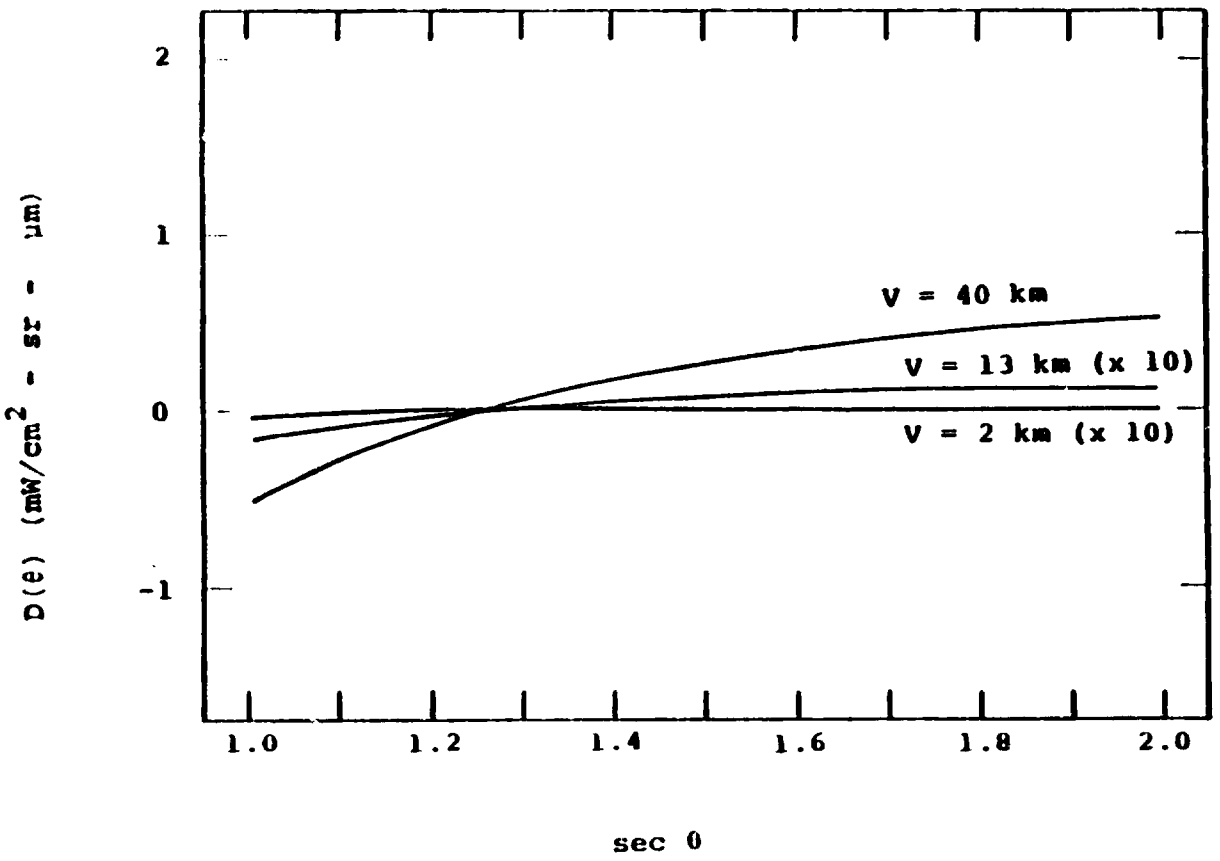

FIGURE 42. VARIATION OF THE DIFFERENCE FUNCTION WITH THE SECANT OF THE NADIR VIEW ANGLE FOR THREE UNIFORM ATMOSPHERES AT A WAVELENGTH OF 0.500 μm.

$\rho_1 = 0.2$

$\rho_2 = 0.25 \cos 0$

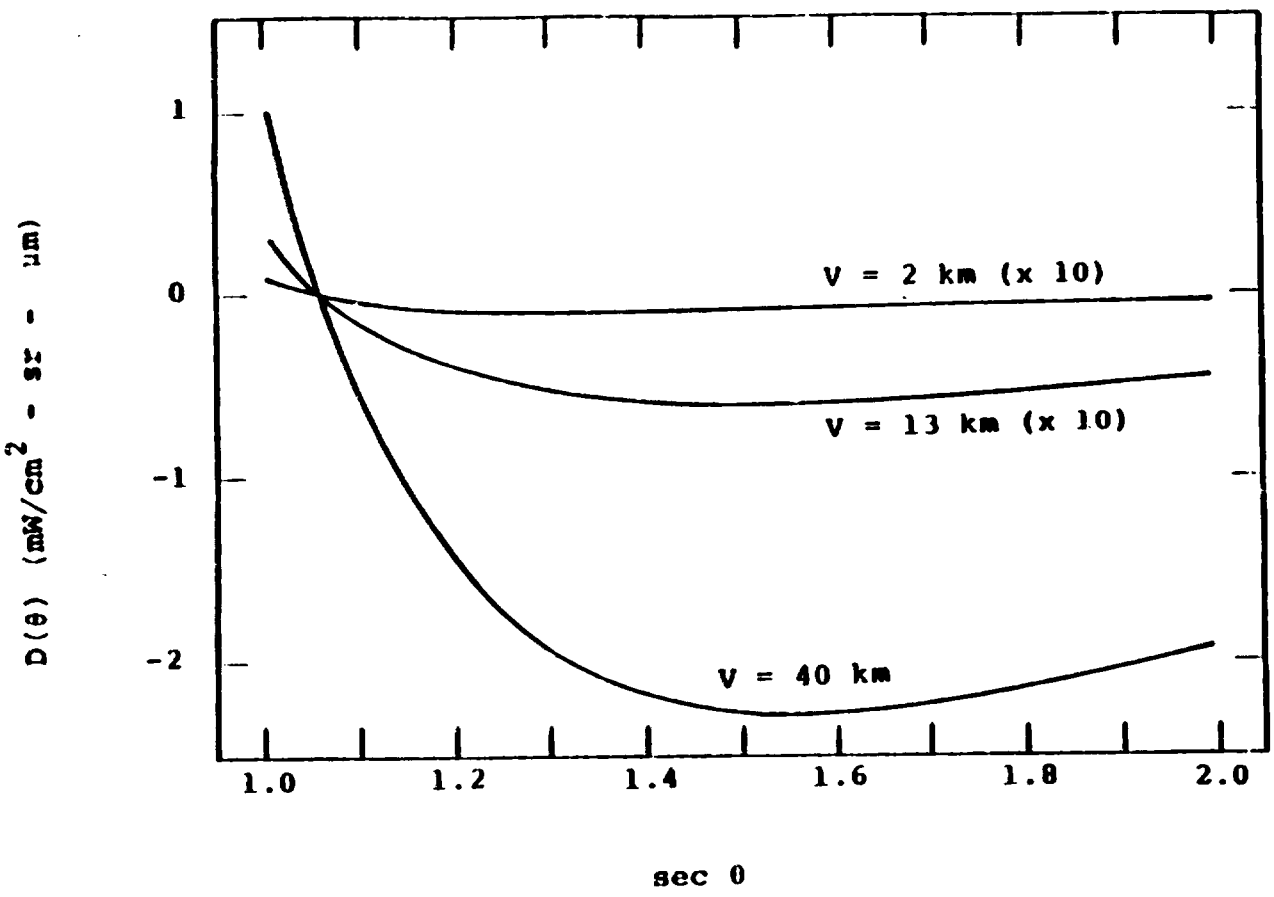

FIGURE 43. VARIATION OF THE DIFFERENCE FUNCTION WITH THE SECANT OF THE NADIR VIEW ANGLE FOR THREE UNIFORM ATMOSPHERES AT A WAVELENGTH OF 0.500 μm.

$$\rho_1 = 0.1$$

$$\rho_2 = \cos 0 \quad \sin^2 \theta$$

variability here is especially pronounced for the high visibility case. Finally, in Figure 44 we present the difference function for a combination of the two targets with angular variations.

From this analysis we have shown that there is enough variability in the angular properties of the targets such that if one knows the geometric characteristics of a target then the spectral transmittance of the atmosphere can be determined from a measurement of the difference function.

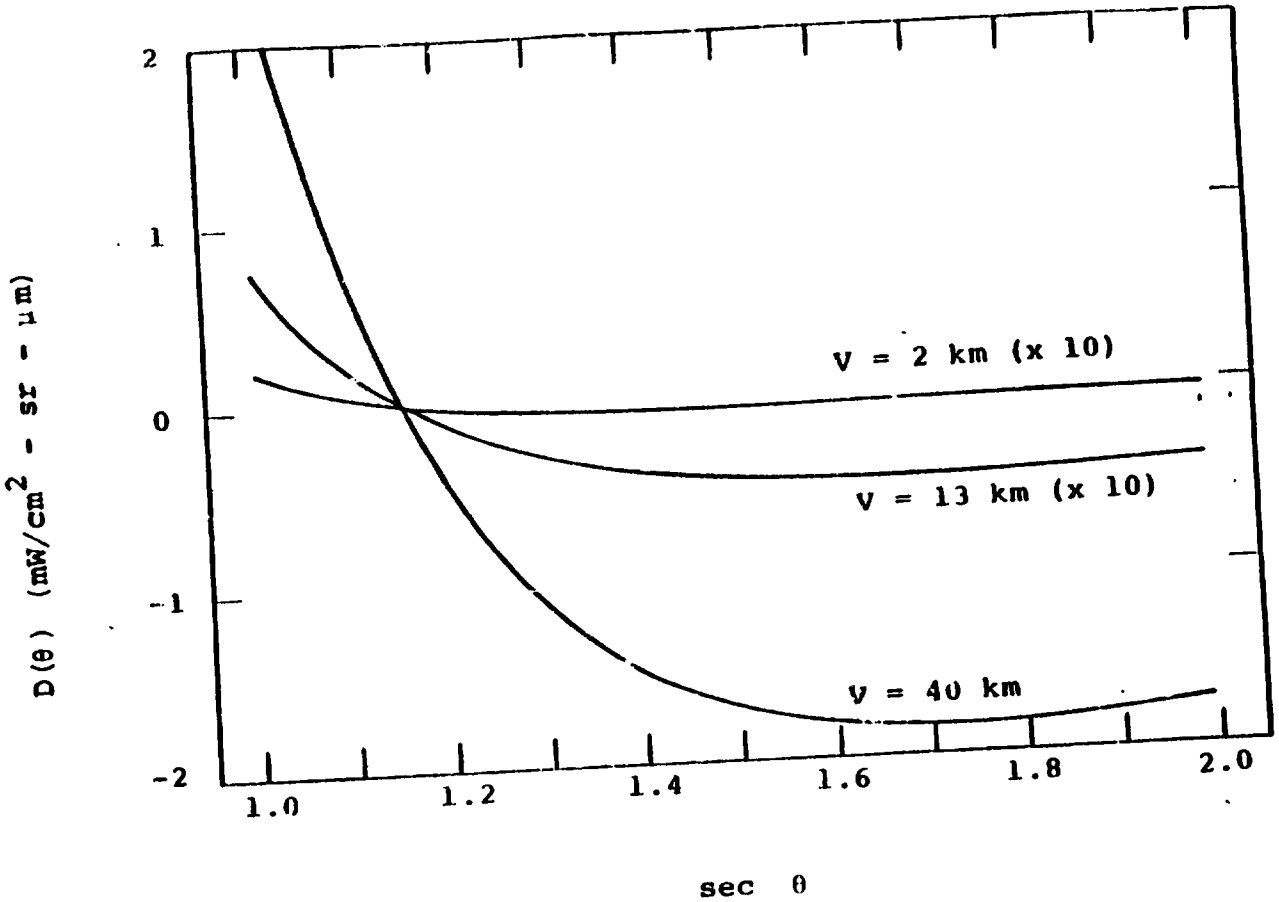

FIGURE 44. VARIATION OF THE DIFFERENCE FUNCTION WITH THE NADIR VIEW ANGLE FOR THREE UNIFORM ATMOSPHERES AT A WAVELENGTH OF 0.500 μm.

$$\rho_1 = 0.25 \cos \theta$$

$$\rho_2 = \cos \theta \sin^2 \theta$$

5
CONCLUSIONS AND RECOMMENDATIONS

In this investigation we have used a radiative-transfer model to simulate the MRS spectral radiances for several atmospheres characterized by various degrees of haze. We also performed the analysis for diffuse (Lambertian) targets and hypothetical targets with quite different goniometric properties. From the resulting radiance diagrams it is obvious that there can be large variations in the radiances depending upon the solar zenith angle, the nadir view angle, the relative azimuth angle, the optical thickness, and the target reflectances.

In terms of its importance to the community of users of remotely sensed data the analysis of the variation of the difference function and transmittance is of greatest utility. Here we found a totally unexpected result, that is, the non-linear change in the transmittance as a function of view angle for inhomogeneous atmospheres and also the non-uniform change in the difference function for the hypothetical targets with various goniometric properties. If one knows the goniometric properties of selected targets, then a measurement of the difference function by the MRS yields the spectral transmittance of the atmosphere. Conversely, if one knows the spectral characteristics of the atmosphere a measurement of the difference function allows one to determine the difference in the angular properties of the two targets. In addition, if one of the targets is known then the other is determined.

Polarization has not been included in the present study. It is generally believed that polarization is not important because of the depolarization characteristics of the atmospheric particulates, expecially for very hazy atmospheres.

From this preliminary analysis we have learned many things concerning the change in radiance for inhomogeneous atmospheres and non-Lambertian targets. Before the MRS sensor becomes "operational" however, we suggest that several additional studies be undertaken so that necessary design modifications can be made in the instrument prior to launch.

First, one should produce more diagrams of the simulated radiances for realistic targets with goniometric and radiometric properties which are characteristic of known natural materials and also for atmospheres with various amounts of absorptive aerosols. In this way one can simulate the MRS radiances for different classes of materials and atmospheric air masses. Thus, one might, for example have radiances for black soil in an urban area of vegetation in a rural area. Certain areas may serve as calibrated test targets for atmospheric correction.

Second, the variation in transmittance with view angle for inhomogeneous atmospheres was surprising. It is now important that the haze gradient be specified for known environments characteristic of urban, rural, coastal, etc. areas. Measurements should be made to determine the haze gradients. Also, one should model hazes more general than the simple "linear visual range" haze considered in this report. The derivative or slope of the transmittance plots could also provide information on the optical thickness for various points in a given area. Hence, the derivative of the transmittance function should be plotted.

Third, we have seen how information can be obtained on the goniometric properties of surfaces if we know something about the atmosphere. One should definitely use realistic bi-directional reflectance distribution functions with inhomogeneous atmospheres to calculate the difference function for the two target radiances for the MRS spectral bands in order to determine the sensitivity of the MRS radiances for various targets.

If these tasks are undertaken then a definite assessment can be made of the potential uses of the MRS for atmospheric correction of remote sensor data. In addition, a whole new remote sensing technique may result for the classification of Earth resources based upon their goniometric properties as well as their spectral characteristics.

REFERENCES

1. Chandrasekhar, S., Radiative Transfer, Dover Publications, 1960

2. LaRocca, A.J. and Robert E. Turner, "Atmospheric Transmittance and Radiance: Methods of Calculation", An IRIA State-of-the-Art Report, 107600-10-T, Environmental Research Institute of Michigan, 1975.

3. Turner, Robert E., "Earth-Atmosphere Albedo Relationships for Realistic Atmospheres", paper presented December 1976 to ODU-NASA/Langley Research Center, Interactive Workshop & Topical Meeting of Optical Society of America, "Atmospheric Aerosols, Their Optical Properties and Effects", to be published in 1977.

4. Turner, Robert E., "Atmospheric Effects in Remote Sensing", Remote Sensing of Earth Resources, Volume II, F. Shahrokhi, Ed., 1972.

5. Turner, Robert E., "Radiative Transfer in Real Atmospheres", Final Report, 190100-24-T, Environmental Research Institute of Michigan, 1974.

6. Turner, Robert E., William A. Malila, Richard F. Nalepka, Frederick J. Thomson, "Influence of the Atmosphere of the Atmosphere on Remotely Sensed Data", Proceedings of the Society of Photo-Optical Instrumentation Engineers, Vol. 51, 1975.

7. Turner, Robert E., "Elimination of Atmospheric Effects From Remote Sensor Data", Proceedings of the Twelfth International Symposium on Remote Sensing of Environment, Center for Remote Sensing Information and Analysis, Environmental Research Institute of Michigan, 1978.

8. Coulson, K.L., J.V. Dave, and Z. Sekera, "Tables Related to Radiation Emerging from a Planetary Atmosphere with Rayleigh Scattering", University of California Press, 1960.

9. Ivanov, A.I., "Atmospheric Optics", Ed. by N.B. Divari, consultants Bureau, New York, 1969.

10. Herman, B., and Robert E. Turner, "The Infrared Handbook, Atmospheric Scattering", Chapter IV, USGPO, 1978.

11. Schnetzler, C.C., and L.L. Thompson, "Multispectral Resource Sampler: An Experimental Satellite Sensor for the Mid-1980's", Proceedings SPIE Technical Symposium, Huntsville, AL, May, 1979.

12. Elterman, L., "Vertical-Attenuation Model with Eight Surface Meteorological Ranges 2 to 13 Kilometers", AFCRL Report No. 70-0200, Air Force Cambridge Research Laboratories, Bedford, Mass., March, 1970.